IEEE Access
Multidisciplinary ⋮ Rapid Review ⋮ Open Access Journal

Received 30 January 2023, accepted 12 February 2023, date of publication 16 February 2023, date of current version 23 February 2023.

Digital Object Identifier 10.1109/ACCESS.2023.3246161

SURVEY

THz Channel Sounding and Modeling Techniques: An Overview

ANIRBAN GHOSH[1,2], (Member, IEEE), AND MINSEOK KIM[1], (Senior Member, IEEE)
[1]Graduate School of Science and Technology, Niigata University, Niigata 950-2181, Japan
[2]Department of Electronics and Communication Engineering, SRM University AP, Amaravati, Andhra Pradesh 522240, India

Corresponding author: Minseok Kim (mskim@eng.niigata-u.ac.jp)

This work was supported by the National Institute of Information and Communications Technology (NICT's) Innovative Information and Communication Technology Research and Development Commissioned Research Beyond 5G Seeds Creation Program under Grant 02701.

ABSTRACT As the world warms up to the idea of millimeter wave (mmWave) communication and fifth generation (5G) mobile networks, realization slowly dawns that the data rate, latency, throughput, and other performance metrics that are used to assess a new wireless communication technology will not be enough to support the demands of envisioned futuristic applications. Thus there is an eagerness to further climb up the frequency ladder to use the large swathes of available spectrum in the $0.1 - 10$ THz band which is expected to act as the key technology enabler to fulfill the requirements of the sixth generation (6G) wireless communication and possibly even beyond. Channel measurement and modeling are crucial to the design and deployment of future wireless communication systems and researchers across the globe are putting their best foot forward to accelerate the process. The current article presents comprehensive assimilation of research efforts in the context of THz channel sounding. A detailed overview of the current channel sounding techniques is first introduced followed by their relevance to THz band channel measurement. An in-house novel channel sounder developed for THz band measurement is also briefly introduced in this context. The paper next provides elaborate dissemination of various measurement campaigns in the band of interest followed by the modeling techniques that are available in the literature and are being adopted for the THz band. Post the description of different challenges and future research directions in the context of sounding, measurement, and modeling the article is concluded.

INDEX TERMS Terahertz communication, channel sounder, channel measurements and characterization, channel modeling.

I. INTRODUCTION

With an exponential growth in smart devices and subsequently the traffic produced by them, the demand for data rate has doubled every 18 month [1] and there is no visible sign of either of them abating. In such a scenario the THz band, which in this manuscript will be considered as frequencies between $0.1 - 10$ THz looks like a promising candidate being an upgrade on the shortcomings of the millimeter wave (mmWave) band in terms of data rate and bridging the gap with optical frequency range. The current demand for high-speed data can only be partially met by using mmWave frequencies in coherence with further improved modulation techniques or sophisticated hardware components. But it is not possible to support the requirements of envisioned applications such as Tera-Wifi, Tera-Internet of Things, Tera-backhaul access, ultra-broadband space communications, nano-networks for molecular communications [2], and similar futuristic applications demanding data rates to the tune of hundreds of giga-bits-per-seconds (Gbps) or even tera-bits-per-seconds (Tbps). Free space optical (FSO) communication on the other hand can provide the necessary data rate and even more due to the availability of large swathes of bandwidth (BW) in the optical range but is heavily affected by unpredictable environmental conditions [3], suffers from high background noise and has limitations in beam tracking [4].

The associate editor coordinating the review of this manuscript and approving it for publication was Mohammad Tariqul Islam.

This calls for a middle-ground approach by using the bridging frequency range between the two extremes, viz. the THz frequencies.

In wireless communication, a channel is a medium that facilitates the propagation of signal between the transmitter (Tx) and the receiver (Rx) using a band of frequencies under investigation. The propagation through a channel is majorly dependent on the channel characteristics and to a lesser extent on transmission techniques as well as hardware components. Thus it is imperative to study and analyze the channel properties at a given frequency so that efficient techniques can be developed to derive the most out of the spectrum of interest and the story is no different when it comes to THz band propagation [5], [6]. The characteristics of a wireless channel are studied by conducting measurement campaigns in different scenarios using a channel-sounding technique where a known signal transmitted from the Tx after being modified and corrupted by the propagating medium is received by an Rx. The received signal is then analyzed to detect the effect of a channel on the propagating signal, extract various channel parameters required to characterize the channel, and generate a model capturing the nature of wave propagation within reasonable complexity.

Several survey papers have focused on studying mmWave channels from the perspective of difference with centimeter wave (cmWave) channels [7], a summary of channel measurements [8], [9], [10], [11], a review of channel propagation [12], [13], sounders [11], [12], modeling [9], [10], [11], [13], and future directions [10], [11], [14]. In summary, the mmWave channel has been extensively studied and its various aspects have been summarized through several survey papers as mentioned earlier. But it would be unwise to simply extend those sounding techniques to study the THz band channels due to constraints on hardware components being used [15]. In addition, a THz band channel can behave very differently from mmWave or other lower frequency channels due to their smaller wavelength which makes the effect of scattering due to surface roughness and scattering and absorption by molecule-level tiny particles such as grains of dust or raindrops, etc. more significant. The small wavelength also provides an advantage by making the design of a large-scale antenna array a reality that can significantly improve channel capacity at the cost of an increase in complexity of modeling a THz band propagation channel which needs to capture the non-stationarity in spatial, temporal, and frequency domain over the array. There is no dearth of surveys on sixth generation (6G) networks [5], [6], [16], [17], [18] and THz communications [19], [20], [21] but those papers mostly delve into system innovations [16], [17], [18], applications suited to the THz band [16], [17], signal processing techniques [22], beamforming [23], imaging [24] and localization [25] in the said band. Furthermore, surveys in the band of interest provide insights on a plethora of topics such as channel modeling and characterization [5], [26], [27], security [19], hardware and system innovation [19], [20], [21], different available simulators [27], their unique requirements [28], standardization activities [26], [29] and research issues and future challenges [16], [27], [28] to least a few. However, a comprehensive overview of all aspects of any wireless

TABLE 1. Summary of relevant surveys.

Year	Reference	Contributions
2010	[19]	Reviews sub-THz and THz communication from the perspective of security, hardware, and implementation.
2011	[20]	Reviews emerging technologies and recent developments in devices that can support ubiquitous THz communication.
2014	[21]	Details the communication and device design challenges at the THz band.
2014	[26]	Provides a synopsis of THz channel modeling, spectrum regulations, and standardization activities.
2018	[23]	Provides an overview on beam control for THz band communications and discusses noteworthy experimental demonstrations.
2018	[24]	Highlights the relevance of THz imaging and emphasizes its impact on both sciences and applications.
2019	[18]	Details on the evolution of networks for 6G implementation with an emphasis on network architecture and enabling technologies.
2019	[29]	Summarises opportunities, challenges, and rulings of regulatory and standardization bodies and illustrates the viability of several applications in the frequency range $0.1 - 3$ THz.
2020	[5]	Provides a review of channel measurements, characteristics, and modeling at mmWave, THz, and the optical band for specific scenarios.
2020	[17]	Elaborates on the paradigm shift and the enabling technologies for 6G communication networks.
2021	[6]	Presents a top-down view of design requirements and proposes changes required in the core network of 6G systems.
2021	[16]	Surveys the technologies, applications, challenges, and research issues in the deployment of 6G networks.
2021	[22]	Overviews THz-specific signal processing techniques with a focus on ultra massive multiple input multiple outputs (UM-MIMO) and reconfigurable intelligent surface (RIS).
2021	[25]	Presents history, and constraints of existing localization methods and a tutorial on THz localization techniques and demonstrates its suitability to 6G communication systems.
2022	[27]	Reviews three popular THz channel sounding techniques followed by a brief review of the corresponding measurement campaigns using the sounders, channel modeling methodologies, channel characteristics, channel simulators, and general open challenges.
2022	[28]	Discusses the requirements and techniques for channel sounding at frequencies between $100 - 300$ GHz followed by a brief overview of channel measurements and general future challenges.
2023	Current work	Provides a detailed overview of four channel-sounding techniques suited for the THz band followed by a comprehensive survey of the measurement campaigns associated with each sounder and different environments. A detailed description of channel modeling techniques applicable to the THz band and future challenges in the context of channel sounding, measurement, and modeling at the THz band concludes the paper.

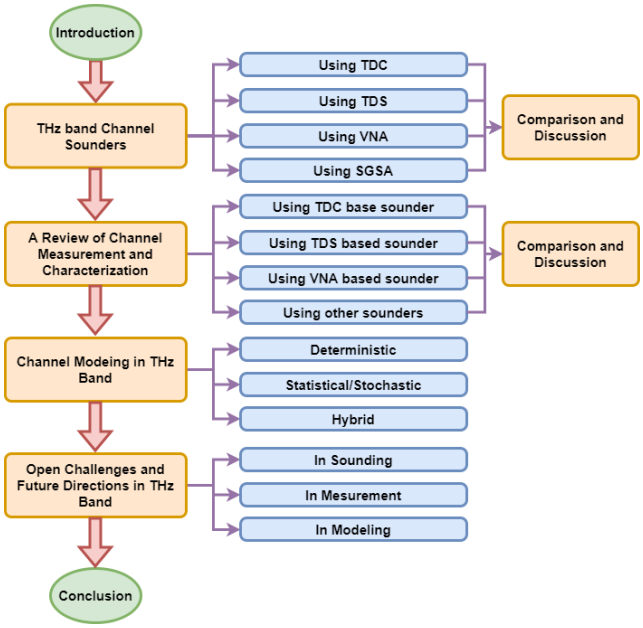

FIGURE 1. Organization of the paper.

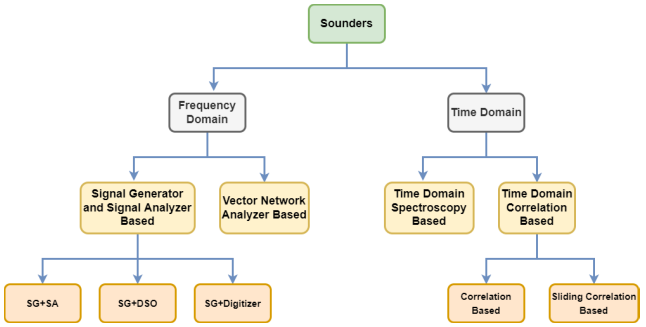

FIGURE 2. Types of Channel Sounder available for THz measurements.

network in a single article is practically impossible, and more so for THz band networks which with their unique set of attributes is still majorly unexplored.

In cognizance of the prior observation, the current work focuses solely on reviewing the state-of-the-art channel sounding techniques, measurement, and modeling for THz communication channels. Such a concentrated approach helps in presenting an exhaustive overview and analysis of the said topics. In addition, a novel and simple channel sounder developed in-house, distinguished by its unique sounding technique never before reported in the context of THz communication is briefly presented in subsection II-D. The main contribution of the article can be listed as follows

- A detailed overview of four major channel sounding techniques available in the literature and their suitability for studying the distinctive THz band channel. A novel in-house channel sounder is also briefly presented.
- An elaborate survey on the various measurement campaigns conducted in the spectrum of interest and their subsequent conclusion from such campaigns. The gaps in such campaigns are also identified.
- A comprehensive dissemination of the available channel modeling techniques and their usage in modeling THz band channels. The assessment of their ease of implementation and appropriateness for characterizing the THz band channels is also undertaken.
- An extensive summary of existing challenges and possible future scope to overcome them in the context of the THz band channel sounding, measurement, and modeling.

The organization of the paper is summarised as shown in Fig. 1. After a comprehensive introduction in section I setting the context of the paper and highlighting its main contributions, section II provides a detailed overview of the different sounders that are being used for THz band channel sounding along with a comparison of their salient features. An elaboration of the different measurement campaigns conducted using the various sounders described in section II is presented next in section III along with a summary of their outcomes. Section IV then deals with the different channel modeling techniques available and identifies the used cases where they have been applied for characterizing a THz band channel. The THz band with its uniqueness and peculiarity provides various challenges which are identified and encapsulated in the context of channel sounding, measurement, and modeling in section V. Furthermore, the gaps in each domain are identified to highlight the future scope of research. The article is finally concluded in section VI.

II. THZ BAND CHANNEL SOUNDERS

A channel-sounding technique essentially involves the transmission of a known signal from the Tx through an unknown channel and its reception at the Rx after being corrupted by the channel. The unknown channel is then characterized based on the knowledge of the transmitted and received signal from different perspectives [30]. The channel sounders can be broadly classified as time domain and frequency domain. The time-domain channel sounders for the band of interest are either built using the Time Domain Correlation (TDC) method or the Time Domain Spectroscopy (TDS) method. The frequency-domain sounders on the other hand are mainly developed using a Vector Network Analyzer (VNA). Another frequency-domain channel sounder comprising a combination of a signal generator and a signal analyzer (SGSA) was earlier thought to be suited for the narrowband (NB) channel measurement [31], [32] but is also currently adopted for THz measurements [33], [34], [35], [36]. A flow diagram of the classification of the sounders available for THz measurements is shown in Fig. 2.

THz band channel sounders should have the capacity to conduct measurements over large swathes of the available BW and should be able to integrate the usage of high gain and directive antennas to compensate for high isotropic path loss and to obtain spatial domain channel characteristics. For

angle or spatial domain channel acquisition which are dual of one another, we primarily depend on the following techniques

- **Full Array** [37] which consists of an array of transmitting and receiving antennas that can operate simultaneously. The method is very fast but expensive and requires complicated calibration due to the requirement of an individual radio frequency (RF) chain for each element in the array.
- **Multiplexed Array** [11] where an array of antennas at the Tx and Rx are controlled by a single RF chain at each end. This method eradicates the shortcomings of the previous method at the expense of an increase in the measurement time.
- **Virtual Array** [38] which comprises of single antenna element at the Tx and Rx. A virtual array is created by physically displacing the individual elements to obtain space domain channel characteristics. The channel is assumed static during measurement using this technique.
- **Directional Angle Scanning** [39] in which single antennas at both Tx and Rx can mechanically rotate to obtain the angular channel response for different values of azimuth and elevation. It is not as fast as the *full array* configuration but also does not suffer from any phase drift that might arise in the case of *virtual array*. The channel is assumed static during measurement and is thus unsuited for dynamic channel measurement.

Each of the channel sounders comes with its fair share of benefits and disadvantages based on the available BW, mobility in the measurement environment, the distance between the Tx and Rx, and the complexity of the sounder. In this section, we elaborate on different channel sounders that are expected to best suit the requirements of THz channel measurement followed by a discussion of their comparative strengths and weaknesses.

A. CHANNEL SOUNDER BASED ON TDC METHOD

A time domain channel measurement holds an advantage due to the fact that the channel impulse response can be directly obtained from the measurements. In that, the correlation-based channel sounder is the preferred choice due to its ease of implementation [40], [41] compared to the other alternative. The sounder is based on the idea of sending a signal from the transmitter end whose auto-correlation is a close approximation of the Dirac delta function [42]. So if a signal $s(\tau)$ is transmitted through a channel with impulse response $h(t, \tau)$ then the received signal $y(t', \tau)$ at a particular instant of time t' can be obtained as

$$y(t', \tau) = s(\tau) * h(t', \tau) \tag{1}$$

where '*' indicates the convolution of the arguments and τ represents the delay. On further calculating the cross-correlation of the received signal with the conjugate of the transmitted signal we can easily obtain the channel

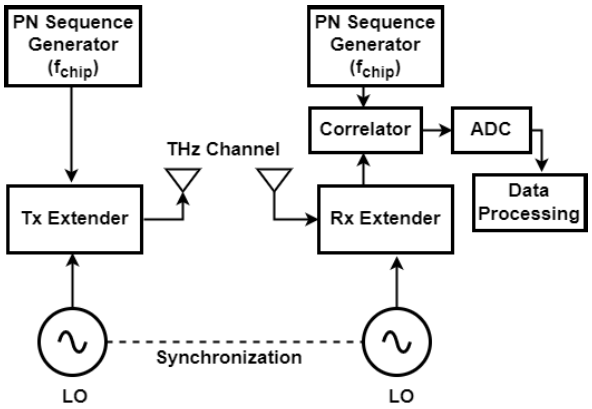

FIGURE 3. Correlation-based channel sounder.

impulse response as follows

$$\begin{aligned} y(t', \tau) * s^*(\tau) &= h(t', \tau) * s(\tau) * s^*(\tau) \\ &= h(t', \tau) * \mathcal{R}_{ss}(\tau) \qquad (2) \\ &\approx h(t', \tau) \qquad (3) \end{aligned}$$

where $\mathcal{R}_{ss}(\tau)$ in equation (2) represents the auto-correlation of the transmitted signal $s(\tau)$ whereas equation (3) follows from the fact that $\mathcal{R}_{ss}(\tau) \approx \delta(\tau)$. As can be observed from Fig. 3 if the modules are not co-located then synchronization between the Tx and Rx module constrains the separation between the modules and their mobility. Thus to overcome any limitations due to synchronization highly stable Rubidium (Rb) clocks are used at the Tx and Rx followed by several hours of a back-to-back (B2B) calibration [43], [44].

In a typical correlation-based sounder a pseudo-random binary sequence (PRBS) also known as a pseudo-noise (PN) is normally used as the transmit signal in which the maximal-length sequence is particularly popular [45]. The binary sequence is passed to a Tx Extender which also receives the signal from the local oscillator (LO) as its other input as shown in Fig. 3. The Tx Extender comprises frequency multipliers, a harmonic mixer, a bandpass filter (BPF), and a power amplifier. The received signal first passes through an Rx Extender which has similar components as its transmitter counterpart to convert the signal to baseband or intermediate frequency (IF) band as the case may be. A PN sequence identical to the one used at the transmitter is used as one of the inputs to the correlator while the output of the Rx Extender serves as the other input. The output of the correlator is passed to a computer via an analog-to-digital converter (ADC) for further processing of the obtained data. This particular setup works quite well for narrowband measurements but for wideband measurements like in the THz band, there is a potential problem. As per Nyquist's Sampling Theorem for properly digitizing the received signal the sampling rate should be at least twice the signaling rate. Due to the wide available BW in the THz band, the signaling rate increases, leading to the requirement of high-speed ADCs, entailing more cost and complexity [45]. The solution to the problem

above lies in slightly modifying the receiver in Fig. 3 by adding a low pass filter (LPF) at the output of the correlator or input of the ADC. The PN sequence at the modified receiver uses a chip rate f'_{chip} which is less than the chip rate f_{chip} of the transmitted sequence. Such an approach leads to the implementation of what is known as a sliding correlation channel sounder where there is a trade-off between the measurement duration and sampling rate [31] and was first introduced in the context of cellular measurement in [46]. Mathematically speaking the channel impulse response gets expanded by a sliding factor $\gamma = \frac{f_{\text{chip}}}{(f_{\text{chip}} - f'_{\text{chip}})}$ which creates a dual effect of reducing the sampling rate and improving the signal to noise ratio (SNR). The Tx of the sliding correlation-based sounders resembles that of the normal correlation-based sounders as shown in Fig. 3. At the Rx, the slower version of the same PN sequence as the Tx is passed as input to the correlator which uses the demodulated received signal as the other input. The output of the correlator is then passed through the chain of low pass filter (LPF) and ADC before being given as input to a data processing unit like a computer.

B. CHANNEL SOUNDER BASED ON THZ TDS METHOD

The other time domain channel sounder using laser pulses enjoys the advantage of possessing huge scalable BW [47] and extremely high speed of channel acquisition [27]. In this sounder, very short-duration pulses having a period greater than the maximum excess delay of the channel is used for transmission. The measured channel impulse response at a particular channel instant t_0 is obtained as

$$h_{\text{meas}}(t_0, \tau) = x(\tau) * h(t_0, \tau) \tag{4}$$

where $x(\tau)$ represents the short laser pulse whereas $h(t_0, \tau)$ represents the actual channel impulse response (CIR). Now as the optical pulse has a much shorter duration compared to the THz pulse, $x(\tau)$ can be approximated by a Dirac delta function and $h_{\text{meas}}(t_0, \tau)$ as $h(t_0, \tau)$. A more detailed derivation of the general transfer function can be found in [48]. The sounder however suffers due to its massive setup and low output power which limits the measurement distance where the second problem is partially alleviated by the usage of a proper lens at both the Tx and Rx. Due to its prior mentioned limitations, this kind of sounder is more suited for the study of reflection, diffraction, and scattering characteristics of materials in the THz band [49], [50], [51], [52].

The architecture of a TDS-based channel sounder consists of a femtosecond laser, a beam splitter, a THz emitter, a mechanical delay line, and a THz receiver/detector [48] as shown in Fig. 4. The femtosecond laser generates the short-duration laser pulse which is given as input to the beam splitter. As the name suggests it splits the input beam into two portions one of which is fed as input to the THz transmitter which has the DC bias as its other input. The DC bias facilitates the separation of the optical pulse from the THz one before it is transmitted. The other portion of the split beam is given as input to the THz receiver/detector after passing through the delay line which helps in the detection of the received THz signal. The detection is dependent on the precise simultaneous arrival of the optical beam and the THz signal at the detector. The computer-controlled mechanical delay line is scanned for its entire path length to obtain the precise temporal delay. The detected signal is further passed through an amplifier before being set as an input to the data processing unit.

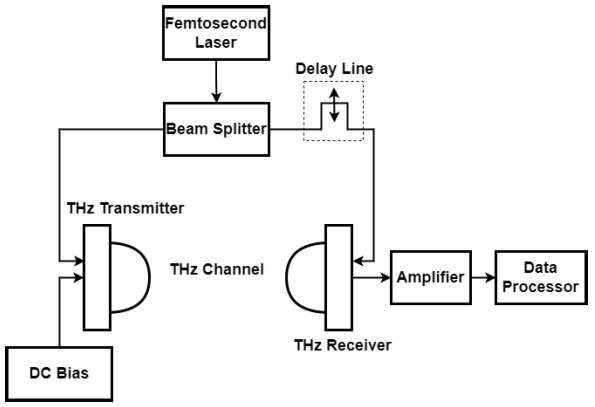

FIGURE 4. Architecture of THz-TDS channel sounder.

C. CHANNEL SOUNDER USING VNA

The frequency response of a channel under test (CUT) can be easily obtained by evaluating the ratio of the signal received at the Rx after passing through the channel to the signal transmitted from the Tx. In the case of VNA, it measures the complex scattering parameter (S-parameters) of the device under test (DUT) where if the DUT is a wireless channel then S_{21} resembles the channel transfer function (CTF) [42]. As the excitation signal sweeps through the band of frequency of interest the CTF is obtained which can be expressed as [28]

$$S_{21}(f) = H_{\text{sys}_{\text{Tx}}}(f) H_{\text{ant}_{\text{Tx}}}(f) H(f) H_{\text{ant}_{\text{Rx}}}(f) H_{\text{sys}_{\text{Rx}}}(f) \tag{5}$$

where $H_{\text{sys}_{\text{Tx}}}(f)$, $H_{\text{ant}_{\text{Tx}}}(f)$, $H(f)$, $H_{\text{ant}_{\text{Rx}}}(f)$, and $H_{\text{sys}_{\text{Rx}}}(f)$ represent the Tx system response, the transmit antenna response, the channel response, the receive antenna response and the receiver system response respectively. After suitable calibration, the system responses and the antenna responses can be compensated to obtain the channel response. Once the channel frequency response is obtained a simple inverse Fourier transform (IFT) produces the CIR.

Due to ease of design, ability to cover large BWs, and simple calibration technique VNA finds wide acceptance among researchers as the choice of instrument to be used for building a channel sounder. However, it is not without its fair share of disadvantages [27] such as (1) low output power, (2) high noise figure, and (3) generally slow sweeping operation. In the context of THz channel sounding the first two problems can be addressed by the usage of proper amplifiers but the third problem is starker since THz channels are known for their channel variation. The consequence of such

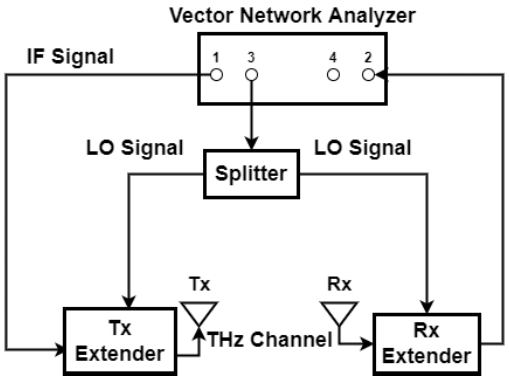

FIGURE 5. Architecture of a VNA-based channel sounder.

limitations means that VNA-based sounders are not suitable for highly dynamic measurement sites.

The schematic diagram of a THz band channel sounder built using a VNA is shown in Fig. 5. The maximum frequency range that a commercial VNA can cover is 110 GHz [53] which is not sufficient to conduct measurements across the THz band. Hence, typically a frequency extender is added at the Tx and Rx side to up-convert and down-convert the signals to the desired frequency range. The frequency extenders can be a commercial one [54] or an assembled combination of power amplifiers, harmonic mixers, and BPFs on the transmit side and a combination of a similar mixer and LNA on the reception end. The signal produced from port 3 as shown in Fig. 5 is split and serves as the LO signal for both the Tx and Rx. In the case where a 4 port VNA is not available, an external frequency synthesizer can be used to provide the LO signal where port 1 of the VNA produces the transmit IF signal and port 2 receive the IF signal after down-conversion. As signal processing at both ends is stationed inside the same instrument, the measurement distance is majorly limited by the cable loss of the co-axial cables connecting the ports to the Tx and Rx modules. A recent solution in [55] using radio frequency over fiber (RFoF) to replace the coaxial cable link connecting the LO signal to the frequency extender on the Rx side showed improved results for increased Tx-Rx separation upto 100 m.

D. CHANNEL SOUNDER USING SGSA

Although this frequency domain channel sounder is deemed more suited for narrowband channel measurements it has been successfully used in several measurement campaigns for the THz band [33], [35], [36], [56]. The sounder known for its simplicity and ease of setup does require an extensive amplifier and multiplier chain (AMC) and filter(s) to transmit signals in the THz band. Such an elaborate setup can lead to erroneous measurement results in the absence of proper calibration to compensate for the effect of system responses. The effect is more prominent in comparison to other sounders. The CTF after proper calibration at a particular frequency is

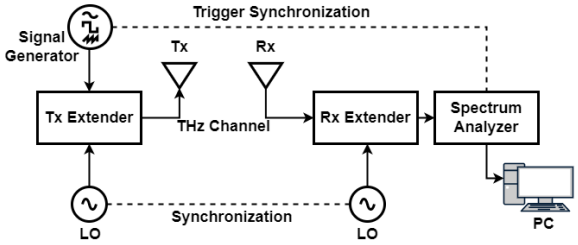

FIGURE 6. Architecture of a channel sounder using a combination of signal generator and spectrum analyzer.

given by

$$H(f) = \frac{Y(f)}{Y_{\text{calib}}(f)} \cdot \frac{G_{\text{Att}}}{G_{\text{T}_{\text{ant}}} G_{\text{R}_{\text{ant}}}} \tag{6}$$

where $Y(f)$ and $Y_{\text{calib}}(f)$ represent the frequency domain response of the received signal during measurement and calibration respectively. G_{Att} represents the attenuation of the attenuator for B2B calibration or free space path loss at reference distance for over-the-air (OTA) calibration. $G_{\text{T}_{\text{ant}}}$ and $G_{\text{R}_{\text{ant}}}$ represents the respective gains of the transmit and receive antennas. Even though long-range measurement capability is counted as one of its advantages such measurements would require complete separation of the Tx and Rx module. The segregation comes at the expense of additional equipment and costs to replace all cable-based synchronization either between the LOs or between the signal generator and spectrum analyzer. Global positioning system (GPS)-assisted synchronized Rb clock [57] or high precision Synchronomat based on Rb clocks [58] is used for synchronizing the LOs at the two ends. In addition, high-precision LO consisting of phase-locked dielectric resonator oscillators can be used in place of the internal clocks of the standard LOs [11]. The internal trigger pulses of the signal generator (SG) and the spectrum analyzer (SA) are synchronized using a direct cable connection during calibration but separated during actual measurement [57]. However, during long measurements, the Rb clocks or the trigger pulses of the SG and SA might fall out of sync and hence the synchronization procedures have to be repeated. While replacing the Rb clocks with the more expensive Cesium clocks having smaller trigger offset rates resolves the synchronization issue of the clocks, using carefully designed data frames with inherent synchronization addresses the issue with trigger pulses.

In order to transmit in the THz band, a pair of extenders are used in both the transmit as well as the receive module as shown in a typical architecture of the sounder in Fig. 6. Wideband unmodulated multitone signals with constant envelope such as Newman phase multitone (NPM) [11] or multi-carrier orthogonal frequency division multiplexing (OFDM) waveforms are usually used as sounding signals by the SG [33], [36]. The signals from the SG and the LO are combined inside the Tx extender which also comprises a chain of frequency multipliers, one or more amplifiers, filter(s), and a mixer not necessarily in the same order to transport

TABLE 2. Comparison of channel sounders.

Type of Channel Sounder	Domain	Measuring BW	Dynamic Range	Measurement Distance	Synchronization	Other Points
TDC Based	Time	Small (no more than 10 GHz)	High	Upto hundreds of meters	Complex synchronization for long distance	Complex design, expensive but can support scalable antenna configuration
TDS Based	Time	Very Large (in THz)	Low	Few centimeters (limited by pulse power)	Easy synchronization due to short distance measurements	Large setup, lack of standardization
VNA Based	Frequency	Large (several GHz)	High (can be further improved with RFoF)	Upto few meters (can be improved with RFoF)	No separate synchronization required	Expensive, increased loss due to heavy usage of cables and low speed of channel acquisition
SGSA Based	Frequency	Moderate	Moderate	Can reach upto dozens of meters	Complex synchronization for long-distance	Inexpensive but suffers from additional noise due to extensive AMC

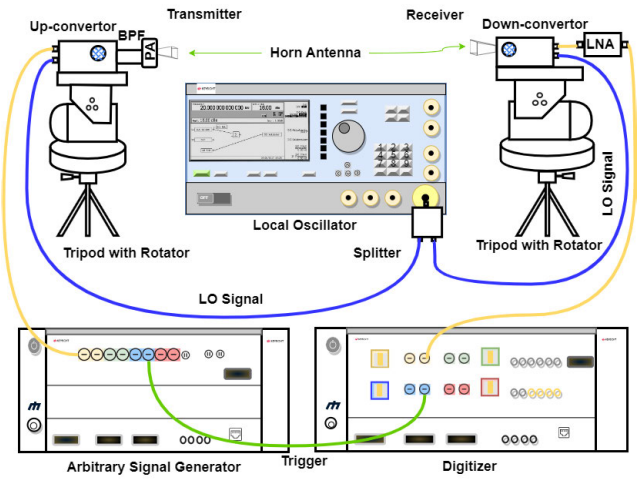

FIGURE 7. Architecture of the novel in-house channel sounder.

the baseband signal to the THz band. As in the case of other THz band sounders, directional antennas are used to compensate for colossal propagation loss. The received signal at the receiver is first passed through an Rx extender comprising components similar to its transmit counterpart but in reverse order to get back the baseband signal which is then captured by the spectrum analyzer. The output from the spectrum analyzer is further processed using a personal computer (PC) to obtain the transfer function and subsequently, IFT of the same gives the CIR. In a variation of this architecture, the spectrum analyzer is often replaced by a digital storage oscilloscope (DSO) [35], [59] or digitizer [34].

A novel in-house channel sounder developed for THz band channel measurement using the same principle but with slight modification is shown in Fig. 7. The modification stems from the fact that usage of extensive AMC causes additional noise which can significantly affect the dynamic range (DR) of the sounder. As can be seen in Fig. 7, the Tx side comprises a LO, an arbitrary waveform generator (AWG) acting as an SG, and an up-converter. The output of the up-converter after passing through a chain of a BPF and an amplifier is transmitted using a directive horn antenna. The Rx side on the other hand comprises a similar horn antenna as on the Tx side, a down-converter that complements the up-converter on the other side, an LNA, and a digitizer that houses a 10-bit ADC. The usage of a digitizer with a 10-bit ADC as against an 8-bit traditional DSO with comparable other features significantly improves the dynamic range. In addition, the digitizer is less expensive than a DSO with similar BW specifications further reducing the cost of building the sounder. For long-distance measurement campaigns, the distance limiting cable connections (blue and green cords in Fig. 2) can be replaced by techniques in [57]. A more detailed description of the sounder can be found in [34].

E. COMPARISON AND DISCUSSION

Calibration forms an integral part of any channel measurement campaign. Even before the start of the actual measurement campaign, a normalization procedure is usually carried out to remove the unwanted effects of the system on the measurement results [60]. The CTF is usually given as $H(f) = \frac{H_{\text{meas}}(f)}{H_{\text{calib}}(f)}$ where $H_{\text{calib}}(f)$ is the CTF obtained using standard calibration procedures of OTA or B2B and $H_{\text{meas}}(f)$ is the original measured response. This measured response can be obtained by using any of the above sounders introduced earlier in the section. However, each sounder comes with its own set of pros and cons which is summarized in Table 2.

The frequency domain response of the CUT can be obtained either with a VNA or a combination of a signal generator and spectrum analyzer (SGSA). The former has the

advantage of implicit synchronization, high time resolution, and simple setup with a single major instrument however it suffers from slow frequency domain acquisition, limited measurement distance, and increased loss due to heavy usage of cables which can be mitigated to some extent by RFoF [55]. The SGSA combination, on the other hand, does not suffer from limitations in measurement distance since the Tx and Rx module can be completely separated at the cost of additional equipment and elaborate synchronization procedure or slower channel acquisition since all the frequency samples are simultaneously transmitted as opposed to sequential sweeping in VNA-based sounding. The measurement BW however is often bounded either by the BW of the sounding signal or the capability of the SG. Furthermore, due to hardware imperfection and noise contribution by different equipment in the elaborate setup coupled with the low power output from an SG, the dynamic range of the sounder is quite moderate compared to VNA-based sounders as evidenced from Table 5 and 6 respectively. As is presented earlier in the section the time domain measurement of a channel also entails two different procedures with their share of advantages and disadvantages. The correlation-based sounders have a higher dynamic range and can support long-distance measurement campaigns and scalable antenna configuration but suffer from complex synchronization for long-distance measurement and often has a complex design which entails higher cost. The laser pulse-based sounders, on the other hand, provide a low dynamic range, are suited for small measurement distances due to limited pulse power, and have a very large setup. Very large measuring BW and easy synchronization can be counted as some of its advantages.

A hybrid approach accounting for the advantages of both methods and neutralizing their disadvantages would be the ideal way forward. In [61] an integration of wideband correlator mode and real-time spread spectrum mode supported long-distance measurement when operating in the former mode enabling extraction of angular and delay spread while short-range measurements captured the dynamic behaviors such as Doppler and rapid fading characterization when operated in the later mode [62]. In [63] an electro-optic sampling (EOS) method which is a specialized type of TDS and shares a similar application space was proposed as a new measurement strategy. A comparison in measurement strategy using different materials (petroleum jelly or a mixture of petroleum jelly and carbon powder) to fill the hollow waveguide in VNA and a transmission cell in TDS produced a satisfactory agreement in results [64] leading to further evidence of possible interoperability between the methods.

III. A REVIEW OF CHANNEL MEASUREMENTS AND CHARACTERIZATION

In the previous section, we elaborated on the various channel sounders that might be suited to drive measurement campaigns in the THz band. In the current section, we take a deep dive into the available literature to explore the application of the sounding techniques for THz channel measurements. In addition, the measurement results, analysis, and conclusions obtained from such implementations are also presented. The rest of the section is organized as describing the THz channel measurements using the TDC, TDS, VNA-based, and other frequency domain sounding approaches (identified as SGSA-based in the current manuscript) followed by a discussion on the measurement results described.

A. MEASUREMENT USING TDC-BASED SOUNDERS

The TDC-based sounder has been extensively used to not only conduct campaigns in the indoor environment but also in interesting outdoor scenarios. In this section, we first summarize the measurement campaigns conducted by different groups across the world in various indoor layouts.

A hybrid channel sounder comprising of correlation mode and real-time spread spectrum mode was introduced in [62]. The sounder supports the measurement of absolute propagation delay and identification of multipath components with a delay resolution of 2 ns in either of the modes. The correlation mode specifically supports the measurement of long-distance parameters such as delay spread and angular spread for propagation path loss of up to 185 dB. The spread spectrum mode on the other hand was more suited to the measurement of short-range, small-scale temporal parameters, and Doppler with a dynamic range of 40 dB for human blockage. In [61], the authors conducted a measurement campaign in an indoor scenario across the various thicknesses of glass and drywall material at 140 GHz to investigate and compare the penetration loss of the same materials at 28 and 73 GHz. The authors concluded from the study that the penetration loss due to garments and other regular materials might not be insignificant for the THz band as opposed to what is considered in the mmWave band. In [65] the reflection, scattering, and large-scale path loss were measured and modeled for the same materials (drywall and glass) and frequency bands (28, 73, and 140 GHz) as the previous work in the [61]. Some interesting revelations from the measurements were - a linear increase in reflection coefficient with an increase in incident angle for all the frequency bands of interest and a lower reflection loss with an increase in frequency for a fixed angle of incidence. The scattered power however was observed to be much lower compared to the reflected power for all bands and angles under test for smooth surfaces. The path loss exponents and shadow fading parameters were observed to be similar across the three frequencies.

The scattering power reradiated from different materials with varying surface roughness was further investigated in [66] using popular scattering models such as Directive Scattering (DS) [67] and Radar Cross Section (RCS) [68]. The study concluded that knowledge of scattering effects was critical in the accurate development of the channel models for both microwave and THz bands. The reflection and penetration loss in vehicular communications at 300 GHz was investigated in [69] using the correlation-based sounder developed in [70]. The reflection losses from the front, side,

and rear of a regular vehicle were reported from the measurements in addition to the penetration losses from the propagation of a signal through, under, and above the vehicle. The effect of heterogeneity of a vehicle body on both the losses was revealed from the study and the trajectory of the signal seemed to have a profound effect on the magnitude of the loss, an observation which was also noted for regular building materials in [65]. A further extensive measurement campaign characterizing the impulse response, the path loss, and other spatiotemporal parameters at 300 GHz for a vehicular channel was conducted in [71]. The consequence of reflection and penetration loss for various representative single-lane and multi-lane scenarios were identified and reported as follows

- A regular vehicle body can serve as a strong blocker.
- For through the vehicle propagation height of the incident signal assumes significant importance.
- For under the vehicle propagation both separation between the transmitting and receiving vehicle and the height of their respective antennas is crucial.
- Significant reflection loss occurs from the side of the vehicle compared to its rear or front.

A 3-D spatial statistical channel model was developed based on extensive measurements at 28 and 140 GHz in an indoor office environment in [72]. Omnidirectional and directional path loss models and other channel parameters such as the number of clusters, cluster power, and cluster delays along with an indoor channel simulator were also reported in the same work. The distribution of clusters was found to follow a Poisson distribution whereas the intracluster distribution of the multipath was observed to follow an exponential distribution. To facilitate sensing and positioning in a smart factory setting a measurement campaign was conducted in a scatterer-rich factory environment at 142 GHz in [73]. The distance between the transmitter and receiver varied from 6 to 40 cm where the measured power delay profile (PDP), angular spectrum (AS), and root mean square (RMS) delay spread confirmed the rich scattering effect due to the presence of different metal surface in the factory setting. The measurement results in [74] concluded the suitability of wireless communication at 300 GHz in a data center environment. The path attenuation, PDP, and power angular spectrum (PAS) for top-of-rack and intra-rack measurements were evaluated and were found to be in good agreement with the environment geometry.

By upgrading the mmWave correlation-based channel sounder [75] using suitable up and down converters, measurements were conducted at 190 GHz center frequency in a conference room in [76]. The focus of this campaign was on the effect of polarization in beamforming applications. Investigations revealed that an increase in polarization diversity increases spatial diversity and a deterministic modeling approach for polarization is required to avoid overestimation. Some other interesting measurement scenarios include inside a train wagon [77], [78] and from inside to outside of an airplane [79]. In [77] the intra-wagon channel was measured at 300 GHz and validated using extensive ray tracing (RT) simulations. The PDP obtained from measurement data was found to be in good agreement with those obtained from RT simulations. The validated 3-D RT simulator was used for extensive simulated measurements for different deployments of Tx and Rx. The scenarios for 60 and 300 GHz center frequencies were differentiated into line-of-sight (LoS), light-non-line-of-sight (L-NLoS), and deep-NLoS (D-NLoS) depending on the existence of the once reflected rays. On analysis of the area ratio, optimum Tx deployment for each of the scenarios was determined. In addition for 12 different simulated scenarios, the channel was characterized in terms of different parameters which when given as input to the quasi-deterministic radio channel generator (QuaDRiGa) was found to be in good agreement with the RT results. In a transition between indoor and outdoor measurement, the Tx in [79] was placed inside a Boeing 737 while the Rx was outside. The motivation was to measure the attenuation by the window and fuselage of an aircraft at 300 GHz for different angles of departure (AOD) and arrival (AOA) using the sounder in [70]. The results indicated a minimum attenuation of approximately 11 dB by the window for perpendicular incidence of the signal but no specific angular dependency of attenuation could be identified.

Although it is very challenging to conduct THz band measurement in an outdoor environment due to various reasons, the rest of the section elaborates on the correlation-based sounders used for measurement campaigns in various interesting outdoor scenarios. Several measurement campaigns emulating an Urban Microcell (UMi) at 142 GHz were reported in [80], [81], [82], [83] using the sounder of [62] and at 300 GHz in [84] using the sounder in [85]. In [80] rooftop surrogate satellite and backhaul measurement and typical terrestrial UMi measurement was conducted for a Tx-Rx separation of up to 117.4 m. The omnidirectional and directional path loss model for both LoS and NLoS scenarios as well as a foliage loss model were extracted from the measurement data for terrestrial and non-terrestrial links. The study confirmed the feasibility of using THz links at 142 GHz for both mobile and fixed communication in outdoor environments for distances upto 117.4 m. In [82] the Tx was fixed in the UMi environment whereas the Rx was moved along a rectangular route of length 102 m where the separation between consecutive Rx positions was 3 m. The motivation was to investigate the spatial autocorrelation properties of shadow fading and delay spread over distance at 142 GHz. The analysis of the measurement data showed the correlation distance of shadow fading was much shorter for above 100 GHz links compared to those below it, whereas the correlation distance of angular and delay spreads were comparable for both spans of frequencies.

One of the promising applications of THz communication is precise position tracking. In [81], the authors used the measurement data to test a map-based position tracking algorithm in an UMi environment. An extended Kalman Filter (EKF) [86], [87] was used to track the position and velocity

of user equipment (UE) moving along the same rectangular path as described in [82]. A mean accuracy of 24.8 cm at 142 GHz over a total of 34 UE locations in LoS and NLoS with Tx-Rx separation ranging from 24.3 − 52.8 m was reported from the measurement data. Channel spatial statistics such as the number of clusters and cluster power distribution were extracted from the measurement campaign in [83] in an UMi environment at 142 GHz conducted across 28 different location pairs of Tx-Rx. The analysis showed that the number of clusters ranged from one to four in all the measurement scenarios and that beamforming provided better spectral efficiency compared to spatial multiplexing in LoS scenarios. In addition, it was also observed that due to a limited number of spatial clusters two spatial streams provided maximum spectral efficiency in NLoS scenarios. In [84] using the measurement data at 300 GHz channel impulse response, path gain, delay, and angular spread were obtained for LoS scenario upto 30 m Tx-Rx separation as well as for NLoS scenario. The measurement was conducted for a total of 6 Tx-Rx locations (3 LoS and 3 NLoS) where the Tx was fixed and the Rx was moved to 6 different locations and was programmed to rotate in the azimuth plane in intervals of 15°.

Extensive channel measurements were conducted for characterizing train-to-infrastructure (T2I) [88] and train-to-train (T2T) [89] channels and were validated using an RT simulator. Such measurement and validation pave the way for the design and evaluation of THz communication-enabled smart train systems. In [88] the measurement-validated RT simulator was further used for additional measurement results in different realistic measurement setups to characterize the channel in terms of different channel parameters such as path loss, shadow fading, and RMS delay spread to name a few. In the T2T scenario [89] the Rician K-factor and RMS delay spread were evaluated from the measured data and then the RT simulator was used to understand the measurement scenario and gain insights on how the moving trains themselves can influence the channel of interest. Based on the results in [78], [88], and [89] the channel capacity of communication channels using various antenna patterns and under different weather conditions were investigated in [90] for T2I, T2T, intra-wagon (InW), inside the station (InS) and infrastructure-to-infrastructure (I2I) scenarios. Such a comprehensive study provides an insightful understanding of the relevant channels for designing of smart railway system utilizing THz links. A summary of different measurement campaigns using TDC-based sounders is presented in Table 3.

B. MEASUREMENT USING THZ TDS-BASED SOUNDERS

The TDS-based sounder is the preferred choice when it comes to studying the reflective properties of different materials [51], [91], scattering caused by objects in a regular environment [50], [52], in the development of interference model for large node density deployment [92] or in investigating the impact of weather on THz communication [93], [94]. In the sequel, we will first summarize the measurement results from indoor scenarios.

In order to appropriately model the propagation environment to support indoor terahertz pico-cellular communication, it is important to understand the effect of reflectivity of regular materials used in a typical indoor environment [51]. In addition to providing the measurement results using a TDS sounder, the authors in [51] also investigated the impact of frequency-dependent reflectivity and the incidence angle of stratified building materials such as double pane windows and white paint on plaster in the frequency range from 100 to 500 GHz. The same Picometrix T-Ray 2000 TDS sounder was used to further extend the investigation on frequency-dependent reflectivity of three planar samples of plaster, pine wood, and glass using the Fresnel equation in [91]. The frequency of interest was from 100 to 350 GHz and the results were verified by comparing reflection measurements at selected incidence angles.

Kirchoff scattering theory was used to modify the Fresnel equation suitably to capture the effect of surface roughness on reflectivity in [50]. The modified Fresnel equation was validated by the measurement results conducted for three different materials - ingrain wallpaper, and two samples of plaster of different roughness. An RT simulation further emphasized the importance of correctly modeling the surface roughness of materials present in a measurement scenario. In [52] the applicability of the extended Kirchoff scattering method [95] to model the surface roughness of regular indoor materials such as wallpaper and plaster was validated by using angle and frequency-dependent measurements using the same TDS sounder. By including the model in an RT simulation, the coverage map of a typical indoor office scenario was also presented. Based on the modeling of scattering by commonly used building materials such as plaster the characteristics of scattered multipath components like AOA, AOD, time of arrival (TOA), and phase distributions were investigated in a small office scenario in [96]. The dependence of this multipath characteristic on surface roughness was presented. An overview of such measurements to analyze the effect of reflection, and scattering on the signal propagation in indoor scenarios and their corresponding conclusions was provided in [26]. A stochastic model of interference in a dense multi-user indoor scenario was presented by considering the shape of the transmitted signal and experimentally validated using a novel 20 user interference set up in [92]. The study concluded that the interference distribution in a low-density network cannot be considered to be Gaussian but as the density increases such that the number of nodes were much greater than the ratio of symbol to pulse duration the distribution approaches the Gaussian shape.

Measurement using a TDS sounder is not only limited to indoor scenarios. In [93], [94] the impact of weather on the outdoor THz propagation link had been investigated. THz links are known to suffer adversely due to atmospheric weather conditions [19], [97], [98] such as fog [99], [100], dust [101] or atmospheric turbulence [102]. The effect of rain

TABLE 3. Comparison of THz band measurements using TDC-based sounders.

Environment	Ref	Measurement Frequency (GHz)	BW (GHz)	DR (dB)	Ant Type-Gain (dBi)|HPBW	Measurement Features	Key Contributions
Factory Building	[73]	142	1	145	Horn-27|8°	TR Sep: 6.3−39.6 m; Meas pts: 13; Az sweep: 45 points in 8° step	Characterizes the channel in terms of path loss, delay, and angular spread and antenna polarization.
Inside Room	[66]	140	1	145		TR Sep: 3 : 0.5 : 5 m; Incident Angles: 10°, 30°, 60°, 80°	Investigates and validates scattering using well-known models.
	[65]	28; 73; 140		178; 40; 145	Horn-15/24.5; 20/27; 27|30°/10°; 15°/7°; 8°		Develops reflection, scattering, and path loss models from measurement data.
	[61]	140	4	145	Horn-27|8°	TR Sep: 3.9 − 45.9 m; Meas pts: 48; Az sweep: 8 points in 8° step/position	Reports indoor propagation and penetration measurement results for common materials.
Indoor office Space	[72]	28; 142	0.8; 1	152; 145	Horn-15; 27|28.8°; 8°		Presents a 3-D spatial statistical channel model for the said frequencies.
Representative set up	[69]; [71]	300	8	60	Horn-26.4|8.5°	TR Sep: 2 − 29 m; Tx/Rx height: 0.4/0.78/1.3 m; Az sweep: 0° : 8° : 88°	Characterizes vehicular channels using measurement data for different scenarios.
Data Center	[74]					Tx/Rx height: 1.5/2.1/2.5 m; Az sweep: full in steps of 8°	Presents measurement data in terms of path loss, PDP, and PAS.
Conference Room	[76]	190	7.5	72	Horn-35|15°	Meas pts: 6; Az sweep: −189° : 15° : 165°; El sweep: −30° : 15° : 30°	Characterizes signal propagation for channel modeling and beamforming application.
Intra Wagon	[78]; [77]	60; 300	8	> 30	Horn-15|30°	TR Sep: 5.34 m; Az sweep: full in steps of 10°	Parameterizes intra-wagon scenario using measurement data and extensive RT and QuaDRiGa simulation.
Indoor to Outdoor of Aircraft	[79]	300	8	60	Horn-26.4|8.5°	TR Sep: 0.9 m; AOD: {270°, 280°, 293°}; AOA: 70° : 8.5° : 115°	Investigates attenuation caused by window and fuselage of an aircraft for different AOD and AOA.
Urban Microcell	[80]	142	1	145	Horn-27|8°	TR Sep: 12.9 − 117.4 m; Meas pts: 28	Presents models for outdoor terrestrial and non-terrestrial channels.
	[83]						Introduces a MIMO channel generation procedure and reports spatial statistics from measurement data.
	[81]					TR Sep: 24.3 − 52.8 m; Meas pts: 34 (Tx fixed)	Tests a map-based position location algorithm.
	[82]						Presents results to augment the development of a spatially consistent channel model.
	[84]	300	2	> 60	Open waveguide(OW); horn-6; 20|90°; 15° (Az), 90°(El)	TR Sep: 6.6−34.1 m; Meas pts: 6; AOA: −180° : 15° : 180°	Reports path gain, delay, and angle spread from measurement data for LoS and NLoS scenario.
Train to Infrastructure	[88]	300	8	> 30	Horn-15|30°	TR Sep: 5.2 and 6.5 m	Characterizes T2I channel inside a station and develops a quasi-deterministic channel model.
Train to Train	[89]					TR Sep: 5.2 m	Characterizes T2T channel through measurement and ray tracing.
Different Railway Scenarios	[90]					T2I: same as [88], T2T: same as [89], Others: same as [90]	Reports channel capacity in railway scenarios with various antenna types and in varied weather conditions.

Note: Ref - Reference, TR sep - Tx-Rx separation, Az - Azimuth, El - Elevation, Meas pts - Measurement points, HPBW - Half Power Beamwidth, Ant - Antenna, Type - Gain|HPBW: values of Tx/Rx for each attribute, same value for Tx and Rx if '/' missing.

attenuation in the band $0.1 - 1$ THz was presented in [93] in a controlled environment to understand the effect of the size of raindrops and their intensity on signal propagation. A rain chamber was used for the purpose where the separation between the Tx and Rx was kept at 4 m. The power attenuation of the THz pulse due to rain was evaluated using the Mie scattering theory [103] and was found to be in good agreement with the measurement data. In [94] a further review of the impact of weather on THz wireless links and channel impairments caused due to the presence of atmospheric gases (such as water vapor) [19], [97], [104], airborne particles (such as fog particles, oil, and rain droplets) [100], [105], [106], and fluctuation in atmospheric refractive index [99], [101], [107] was presented. A gist of the measurements is presented in Table 4.

C. MEASUREMENT USING VNA-BASED SOUNDERS

VNA is the approach of choice when it comes to the design of channel sounders for THz band channel measurements. The ease of implementation and low complexity has motivated several research groups worldwide to undertake various indoor measurement campaigns using the said method.

In [108] the authors conducted a campaign inside a shopping mall at 28 and 140 GHz to study and compare the difference in their large and small-scale parameters. In addition, the study confirmed that although the strong multipath component (MPCs) structure was similar between the bands, there were a higher number of clusters and paths per cluster in the 28 GHz compared to 140 GHz for the weaker MPCs. Another study on MPC extraction was carried out in [60] for frequency bands $75 - 110$ and $220 - 330$ GHz. A similar inference as in [108] was drawn where there was similarity in dominant MPCs but the lower frequency band seemed to present additional weaker MPCs. In [109], measurement campaigns were conducted for three different frequency bands: $125 - 155$, $235 - 265$, $270 - 300$ GHz in two different laboratories of dimensions $12.9 \times 7.15 \times 4$ m^3 and $9.7 \times 4.73 \times 4$ m^3 respectively for MPC detection, along with clustering of the detected MPCs. In addition, path loss, and delay spread models were reported in this work. Characterization of path loss, delay spread, MPC detection, and clustering was also reported for a D-band channel in a laboratory environment (with usual scatterers), conference room, and ordinary office in [110]. In addition, the inter and intra-cluster models were also reported in this work. In an extension to the study in [108], measurements were conducted in another indoor hotspot (InH), the airport check-in hall [111]. The large-scale omnidirectional parameters from the measurement data were found to be in good agreement with those of the Third Generation Partnership Project (3GPP) for New Radio (NR).

Several measurements were carried out by the group at Georgia Tech. [112], [113], [114] across different frequency bands to study the various characteristics of the channel across frequencies ranging from 30 to 300 GHz in different indoor scenarios. In [113], the different path loss models were compared with the measurement results at 30, 140, and 300 GHz conducted in a laboratory environment. It was concluded, that in the absence of measurement error, all the models produced comparable results, however, multi-frequency models were found to be inherently more stable compared to the single-frequency models. A similar observation was made in [115] where the single band and multiple band path loss characteristics were modeled for both 140 GHz and 220 GHz in a meeting room environment. The measurement campaign in [112] conducted at the D - band investigated the LoS, the reflected NLoS (R-NLoS) with different reflecting objects, and the obstructed LoS (O-LoS) channels with cylindrical obstacles in the same lab environment as in [113]. A single slope path loss model with shadowing was devised for the O-LoS measurement and multipath propagation analysis. Significant reflections from Tx and Rx systems were observed in the case of LoS and O-LoS measurements whereas in the case of R-NLoS glass and ceramic reflectors led to surface-reflected rays. The different statistical characteristics such as path loss, RMS delay spread, the mean excess delay, the maximum excess delay, and the coherence BW of a desktop THz channel at 300 to 320 GHz were evaluated from the measurement campaign in [114] for both LoS and NLoS. It was observed that metal reflectors produce multiple significant reflecting paths adding to the propagation loss.

Path loss model with shadowing and the effect of different reflecting materials in LoS and NLoS scenarios in a desktop environment were also investigated for the frequency bands: $300-319$, $340-359$, and $380-399$ GHz in [116]. The authors further derived different fundamental parameters that can be used for applications in both macro and micro-scale Internet of Things (IoT). Another study [117] that explored the effect of different reflecting objects to signal propagation was conducted at 300 GHz in a typical desktop scenario. The study further extended the measurement to a small office scenario where the focus was on the identification and characterization of LoS and NLoS paths upto two reflections.

A study of the LoS and R-NLoS paths was carried out in [118] for the 60 GHz wide band between $240 - 300$ GHz to differentiate between the reflections caused by the environment and the setup geometry from the obtained PDP. Other channel parameters such as mean excess delay, RMS delay spread, and coherence BW were also evaluated from the measurement results. The different channel parameters such as path loss, power-delay-angular profiles (PDAP), temporal and spatial features, and correlations among channel parameters were analyzed and determined for a meeting room in [119] and an office room in [120]. The band of interest in both campaigns was $130-143$ GHz. A hybrid channel model was also developed from the meeting room measurement in [121] which was in good agreement with the measured data and was found to be an improvement to the existing geometry-based stochastic channel model (GBSM). Another office environment measurement was conducted [122] for the $140 - 220$ GHz band to characterize the path loss exponent

TABLE 4. Comparison of THz band measurements using TDS-based sounders.

Environment	Ref	Measurement Frequency (GHz)	BW (GHz)	DR (dB)	Ant Type-Gain (dBi)| HPBW	Measurement Features	Key Contributions
Material Surface	[50]	$100-1000$	900	48	Photoconductive antenna +polyethylene lens (PEL) -—|—	AOI: $25°, 30°, 40°, 50°, 60°, 70°$; Thickness: wallpaper-6.5mm, plaster-8.6 mm	Investigates the influence of scattering on specular reflection from rough surfaces.
	[51]	$100-500$	400			AOI: $25°, 30°, 40°, 45°, 50°, 60°$; Thickness: layered glass-7.8mm, white paint-0.695 mm	Presents frequency and angle-dependent reflection measurement and their impact to signal propagation.
	[91]	$100-350$	250			AOI: $20°, 30°, 40°, 50°, 60°, 70°, 75°$; Thickness: glass-2.84mm, plaster-2.74 mm, wood-3.68 mm	Characterizes frequency and angle-dependent reflectivity of common materials.
	[52]	300	10	$7.7-38.1$		AOI: $30°$(fixed); AOR: $0° : 1° : 9°$	Investigates the impact of diffuse scattering from rough surfaces to THz communication.
Representative setup	[92]	$100-4000$	3900	—		Tx position: 27.5 cm from one interferer; Rx position: 14.5 cm from same interferer at an angle of $50°$; Interferers: 20	Develops and experimentally validates a stochastic model for multi-user interference.
Rain Chamber	[93]	$100-1000$	900	—		TR Sep: 1 m; Rain rate: 50 to 500 mm/hr	Investigates effects of rain attenuation to THz communication.

Note: Ref - Reference, TR sep - Tx-Rx separation, AOI-Angle of incidence, AOR-Angle of reflection, HPBW - Half Power Beamwidth, Ant - Antenna.

and the shadowing parameters of the channel. The PDP of the LoS measurement confirmed the presence of negligible multipath for the scenario of interest. The measurement data for the $260-400$ GHz spectrum on a desktop in [123] were analyzed to model the path loss and phase delay for different Tx-Rx separation, angles of arrival, and reflecting objects along with their capacity limits.

Measurement across a large spectrum of 250 GHz from $500-750$ GHz was used to calculate the atmospheric effects on signal propagation in [124]. The CIR for various Tx-Rx separations was acquired and used to present the PDP of the channel. A different kind of measurement campaign investigating the effect of diffraction from objects like edges, wedges, and cylinders on signal propagation at 60 and 300 GHz was reported in [49]. In addition, the shadowing of rays by human beings was also modeled with the help of diffraction where theoretical approaches were validated by measured data.

Due to the inherent complexity involved in measurement across the THz band, most of the campaigns concentrate on single Tx and Rx antenna configuration and in common indoor environments like desktops, offices, laboratories, or conference rooms. However, some literature can be found where multiple input multiple outputs (MIMO) campaigns were conducted, and also other unique measurement environments were explored. A 2×2 MIMO measurement implementation with the virtual antenna array technique was reported in [125] in the frequency range $298-313$ GHz. The authors reported an improvement in the reliability of a 7 Gbps MIMO link compared to a 5.55 Gbps single-channel link. In [126] another 2×2 MIMO measurement campaign in the frequency band $275-325$ GHz was presented where the individual rays are resolved based on the AOA and AOD. An advanced frequency domain RT approach was used to simulate the indoor office scenario used for the measurement campaign and was validated using the measurement data. In contrast to the aforementioned campaigns in a typical indoor scenario (office, desktop), a 4×4 MIMO setup in a data center scenario was studied in [129] to analyze path loss, shadowing gain, RMS delay spread, and Doppler shift.

Several propagation scenarios such as LoS, NLoS, O-LoS, and obstructed NLoS (O-NLoS) were investigated in a data center setting and the channel characteristics such as path loss and RMS delay spread were analyzed in [128]. Cluster-based modeling validated by the measured data at $280-320$ GHz was also implemented. The wireless propagation link for Rack-to-Rack (R2R) and Blade-to-Blade (BTB) in a data center for LoS, NLoS, R-NLoS, obstructed R-NLoS (OR-NLoS) conditions were studied in [130]. A very unique measurement campaign at 300 GHz was conducted on a computer motherboard in [131]. The measurement results indicated optimal communications can be achieved on a motherboard by carefully aligning the antennas with respect to the layout of the board. A measurement campaign in a lecture room exploring the LoS scenario with Tx-Rx separation upto 5 m was reported in [127] for the $300-310$ GHz spectrum. The effect of different antenna combinations at Tx and Rx was investigated and a single slope path loss model was developed from the measurement data. The effect of different antenna types was also studied in [117] in addition to the examination

of interference constellation in accordance with the two-ray model. An application-specific experimental setup demonstrating a 20 Gbps KIOSK instant data downloading system at 300 GHz in an LoS scenario was demonstrated in [132].

As is evident there has been a plethora of campaigns for different indoor and short-distance scenarios. However, when it comes to outdoor measurement to the best of our findings the measurement campaigns [55], [133], [134], [135] initiated to characterize the urban environment are the only results. In [135] the measurement was conducted for maximum separation of upto 15 m in the frequency spectrum of 140 − 141 GHz and analyzed how the channel parameters change as the separation increases. For the mid-range measurement campaign of up to 35 m in the frequency band 145 − 146 GHz, [55], the environment was found to be multipath rich leading to significant delay and angle dispersion. It was further observed that the multipath richness was further enhanced by the usage of metallic covers such as aluminum foil. A measurement with upto 100 m separation between Tx and Rx was conducted in the frequency band 141−148.5 GHz in [133]. The results obtained from the campaign showed the presence of a large number of directions (directions of arrival and departure) with significant energy once again confirming the multipath richness as observed for the mid-range measurement. Finally, an exhaustive measurement campaign consisting of 38 Tx-Rx pair locations with separation ranging from 1−100 m was conducted in [134]. The different channel parameters such as path loss, shadowing, delay spread, angular spread, and MPC power distribution were modeled from the measurement data which pointed toward the feasibility of communication over tens of meters even in NLoS scenarios. There is an acute need for similar outdoor measurement campaigns at similar or different frequency bands of the THz spectrum to understand the fundamental limitation to signal propagation in divergent outdoor scenarios. Table 5 presents a summary of the measurement campaigns conducted using a VNA-based sounder.

D. MEASUREMENT USING OTHER SOUNDERS

Due to their suitability for narrowband measurements, SGSA-based sounders have not been extensively used for measurement campaigns in the THz band. In [33] a measurement campaign was conducted at 350/650 GHz in a typical indoor scenario of a conference room. The path loss and reflection losses were characterized from the obtained data as a function of transmitting and receiving angles. Full azimuth rotation was performed for both the Tx and Rx in intervals of 3°. Several spatially resolvable paths could be associated with the measurement environment. In addition, a propagation model was developed from the measurement data and the importance of NLoS paths for reliable communication in the THz band was confirmed. A similar setup was used in [56] to analyze the reflection characteristics of common indoor materials such as fiberboard, plywood, plastic, plasterboard, and ceramic tile for varying frequency, angle of incidence, and thickness of the material. The CTF obtained from the measurement campaign conducted at 340 GHz in a room was further validated using RT simulation. Measurement campaigns using an SG at the Tx and a DSO at the Rx is also available in literature [35], [36], [59]. The effect of hardware non-linearity on the quality of the received signal was investigated in [35]. The experimental setup illustrated the frequency selective fading of the received signal due to hardware imperfection. The suitability of OFDM was investigated for indoor ultra-wideband THz communication and the optimal parameters of OFDM were extracted to achieve a physical layer data rate of 42 Gbps. In the age of software-defined radio, there was a vacuum in the THz band measurement paradigm in the development of hardware and architecture utilizing the same until [36], [59]. The testbed provides a platform for conducting experimental research in three different bands - 120−140 GHz, 210−240 GHz, and 1.00−1.05 THz. The platform consists of analog front-ends at three different frequency bands and three different digital signal processing back-ends comprising an offline ultra-broadband signal processing engine, a real-time software-defined radio platform, and a radio frequency system on chip (RFSoC) based real-time multi-GHz multichannel digital signal processing engine. A synopsis of the different measurements using the said sounder is presented in Table 6.

E. DISCUSSION

As evidenced from Table 3-6 the measurement environments can be broadly classified as indoor and outdoor. As per the promising applications envisioned for the THz band, it is important to characterize the propagating channels in both environments to provide meaningful insights for real implementations. It is expected that in the THz band in addition to the LoS propagation the NLoS links supported by up to two bounce reflections from common materials are going to be crucial. This has led to a plethora of investigations of the impact of common building materials using TDS-based sounders [50], [51], [52], [91] and VNA-based sounders [49]. THz bands are known to be inherently directive and hence efforts have been invested to study the attributes of directional propagation in several studies [61], [72], [73], [76], [109], [115], [120], [134], [135]. However, such directional campaigns suffer from extensive time requirements which often limit the number of measurement points or time and frequency resolution. To address such challenges and generate extensive data for a massive number of measurement points with tunable resolutions, measurement-validated ray tracing simulators have been developed from different studies [89], [126]. In addition, due to its highly directive nature, communication in the THz band is intrinsically secure. Furthermore, the band is expected to support profound applications in short distances preferably in the LoS environment. Such a requirement motivated investigation of the channel across several THz frequency bands in common indoor spaces such as office rooms [61], [65], [66], [72], [96], [109],

AQ:5 **TABLE 5. Comparison of THz band measurements using VNA-based sounders.**

Environment	Ref	Measurement Frequency (GHz)	BW (GHz)	DR (dB)	Ant Type-Gain (dBi)|HPBW	Measurement Features	Key Contributions
Desktop	[112]	D-band	60	90	Pyramidal horn-22 – 23|9° – 12° (Az), 12° – 13.5° (El)	TR Sep: 35.56 : 5.08 : 86.3 cm; Meas pts: 11/scenario/material; Material: glass, plastic; ceramic (obstruction); aluminum, fiberboard (reflection)	Characterizes D-band indoor channel for different LoS and NLoS scenarios.
	[113]	30; 140; 300	13.5; 60; 16	80	Horn-10|55°	TR Sep: 20 : 5 : 180 cm; same as [113]; 10 : 2.5 : 25 cm	Compares path loss models across different frequency bands.
	[114]	300 – 320	19.99	90	Horn-26|10°	TR Sep: 5 : 5 : 70 cm, 30 cm (diagonal, NLoS); Material: FR4, metal, plastic	Presents statistical characterization of 300 GHz desktop channel.
	[116]	310; 350; 390	19	60	Diagonal horn-23 – 26.5|12°	TR Sep: 5 – 70 cm, 10 cm (fixed), spatial displacement in steps of 30°; Materials: ceiling panel, paint-coated aluminum, copper	Presents statistical channel characterization to compare different bands of THz channels.
	[118]	240 – 300	60	115	Horn-24 – 25|10° (Az), 8° (El)	TR Sep: 40 cm (fixed); AOI: 45° (fixed); Materials: absorber, wood, plastic	Characterizes the multipath channel in terms of various channel parameters.
	[123]	260 – 400	19	60	Diagonal horn-23 – 26.5|12°	TR Sep: 10 – 95 cm, AOA: 0° : 30°; Materials: fiber mat, glass, hand	Characterizes channel for different distances, angles of arrival, and reflectors.
	[124]	500 – 750	250	> 80	Diagonal horn-—|—	TR Sep: 0, 1, 2, 4, 6, 9 inch	Analyzes ultra-wideband measurement data to calculate the atmospheric effect on signal propagation.
	[125]	300	14	—	Horn-25|12°	TR Sep: 25 cm; Array element spacing: 1.2 cm, MIMO configuration: 2 × 2	Presents throughput analysis of 2 × 2 MIMO channel in THz band.
Desktop and Office Room	[117]	300 – 310	9.99	85	OW; horn; horn + PEL-9.9; 26; 39|100°; 10°; 1°	TR Sep: 20 – 100 cm (desktop), 1.67 m (office); Az sweep: −5° : 5°; Materials: glass, fiberboard, flexi-glass, copper	Presents and analyzes temporal channel characteristics for different setups.
Office room	[109]	125 – 155; 235 – 265; 270 – 300	30	105	Horn-20|18°	No. of campaigns: 3 (CM1, CM2, CM3); TR Sep: 7 m (CM1), 7.5 m (CM2), 6.6 m (CM3); Meas pts: 16 (CM1, CM2), 15 (CM3); Azimuth sweep: −180° : 20° : 180° (Tx), −160° : 20° : 160° (Rx)	Presents empirical indoor channel characterization.
	[110]	126 – 156			Horn-20|20°	TR Sep: 10.6 m; Az sweep: −170° : 20° : 170°; Materials: human phantom, plasterboard (11 cm thickness), door (5 cm thickness)	Presents measurement based modeling of D-band indoor channel.
	[120]	140	13	~ 80	Horn-15/25|30°/10°	TR Sep: 2 – 30 m; Meas pts: 74; Az sweep: 0° : 10° : 360° (Rx); El sweep: −20° : 10° : 20° (Rx)	Analyzes channel measurement data from different scenarios in an office room.
	[122]	140 – 220	80	120	Horn-21|13°	TR Sep: 0.5 : 0.5 : 5.5 m; Meas pts: 33	Analyzes measurement data for insight on signal propagation and models path loss in THz indoor scenario.
	[126]	275 – 325	50	65	Horn + PEL-80.1|2°	TR Sep: 1.82, 2.62, 2.90 m; Meas pts: 3; Az sweep: 0° : 2° : 360°; MIMO configuration: 2 × 2	Characterizes channel from spatially resolved and MIMO channel measurement data validated by RT simulations.
Meeting and Office Room	[115]	140; 220	13; 8	~ 80	Horn-15/25|30°/10°	Meas pts: 10; rest same as [120]	Characterizes path loss for THz indoor scenarios.

Note: Ref-Reference, TR sep-Tx-Rx separation, AOI-Angle of incidence, Az-Azimuth, El-Elevation, HPBW-Half Power Beamwidth, Ant - Antenna, Type - Gain|HPBW: values of Tx/Rx for each attribute, same value for Tx and Rx if '/' missing.

TABLE 5. *(Continued.)* **Comparison of THz band measurements using VNA-based sounders.**

Environment	Ref	Measurement Frequency (GHz)	BW (GHz)	DR (dB)	Ant Type-Gain (dBi)|HPBW	Measurement Features	Key Contributions
Meeting Room	[119]	140	13	~ 80	Horn-15/25|30°/10°	TR Sep: 1.8 – 7.3 m; Meas pts: 10	Presents a temporal-spatial analysis of measurement data in an indoor scenario.
	[121]					Meas pts: 21; Az sweep: 0° : 10° : 360°	Develops a hybrid channel model comprising ray-tracing and statistical methods.
Lecture Room	[127]	300 – 310	10	115	Horn; OW-26; 9.7|2.9°(Az), 2.5°(El);46.5° (Az), 130°(El)	TR Sep: 2 : 1 : 5 m	Characterizes THz indoor channel for different antenna directivities.
Data Center	[128]	300 – 320	19.99	—	Horn + teflon lens-22 – 23|10°.The numbers are for horn alone, improvement due to lens not available	TR Sep: 175 cm (LoS, OLoS), 9 cm; Vertical offset: 0 : 1 : 6 cm (LoS); Meas pts: 26 (OLoS)	Presents a comprehensive characterization and modeling of THz channel.
	[129]	300 – 312	11.99			TR Sep: 15, 40 cm; Array element spacing: 1 mm; MIMO configuration: 4 × 4	Introduces a two-dimensional geometrical propagation model with scatterers for a MIMO channel.
	[130]					TR Sep: 40 – 210 cm in steps of 5 and 10 cm and 20 : 1 : 49 cm; AOI/AOR: 20° : 5° : 85°; Materials: cables (obstruction), aluminum (reflection)	Presents statistical channel model for characterization of a 300 GHz channel in the given scenario for different setups.
Computer Motherboard	[131]	300	19.99		Pyramidal horn -22 – 23|10°	TR Sep: 11.7 – 31.7 cm; AOI/AOR: 20° – 80°; Tx/Rx Height: 0 – 2.1 cm; Corridor width: 1.7 – 5.2 cm; Materials: heat sink, fan (obstruction), dual-in-line memory module (reflection)	Characterizes a channel in the said environment for different scenarios.
Shopping Mall	[108]	28; 140	4	123; 130	Bicone/horn-0/19|60°(El)/ 10°(Az), 40°(El)	TR Sep: 3 – 65 m; Meas pts: 18(140), 8(28); Az sweep: 0° : 5° : 360° (Rx)	Compares channel characteristics at two different frequency bands.
Shopping Mall and Airport Check-in Hall	[111]	140		125		Airport: TR Sep: 15 – 51 m; Meas pts: 11; Az sweep: 0° : 5° : 20° and 240° : 5° : 360°; Shopping mall: same as [109]	Estimates large-scale parameters in a quasi-static indoor scenario and compares it with the relevant 3GPP models.
KIOSK	[132]	270 – 340	120	—	Diagonal horn-25|—	TR Sep: 30 : .01 : 32.5, 200 : .01 : 202.5 cm and 10 : 10 : 100 cm	Investigates self-interference due to LoS reflection for indoor short-range communication.
Material Surface	[49]	60; 300	20; 50		Horn; horn/horn+PEL-20; 20/33| —;—/1.5°	TR Sep: 2.7 m (60), 1 m (300), −5 to 9 (translation stage); Angular range: −45° : 1° : 30°; Materials: metal, wood, human body	Investigates the impact of diffraction from materials of different shape along with the shadowing effect of a human body on signal propagation.
Urban Environment	[55]	141 – 148.5	7.5	146	Horn-21|13°	TR Sep: 100 and 104 m; Az sweep: −45° : 5° : 45° (Tx), full in steps of 6° (Rx)	Presents RFoF extended channel measurement and subsequent characterization.
	[133]	145 – 146	1	60		TR Sep: 15.9, 24, 29.9, 34.2 m; Meas pts: 5; Az sweep: same as [55]	Presents channel characterization for LoS and NLoS links and explores the impact of metallic-covered on signal propagation.
	[134]			110		TR Sep: 1 – 100 m (LoS), 2.4 – 100 m (NLoS); Meas pts: 38, Az sweep: full steps of 10°	Characterizes outdoor propagation channel from extensive measurement data.
	[135]	140 – 141		146		TR Sep: 1, 2, 5, 15 m; Meas pts: 4, Az sweep: full in steps of 10°; El sweep: 80° : 10° : 100° (Rx)	Analyzes the changes in channel properties as Tx-Rx separation increases on a linear route.

Note: Ref-Reference, TR sep-Tx-Rx separation, AOI-Angle of incidence, AOR-Angle of reflection, Az-Azimuth, El-Elevation, HPBW-Half Power Beamwidth, Ant - Antenna, Type - Gain|HPBW: values of Tx/Rx for each attribute, same value for Tx and Rx if '/' missing.

TABLE 6. Comparison of THz band measurements using SGSA-based sounders.

Environment	Ref	Measurement Frequency (GHz)	BW (GHz)	DR (dB)	Ant Type-Gain (dBi)|HPBW	Measurement Features	Key Contributions
Conference Room	[33]	350/650	—	—	Horn-25|12°	TR Sep: 0.5 – 10 m; Az sweep: full in steps of 3°	Characterizes path and reflection loss as a function of transmit and receive angle.
Inside Room	[56]	340	40	90	Horn-26|—	Meas pts: 41; AOI/AOR: 0° to 90°; Thickness: fiberboard-4.66 – 15.27 mm, plywood-8.5 – 18.23 mm, plasterboard-12.13 – 12.4 mm, plastic-27.79 – 48.96 mm, ceramic tile- 8.69 – 8.8 mm	Analyzes reflection characteristics of indoor materials such as fiberboard, plywood, plasterboard, plastic, and ceramic tile.
Desktop	[35]	140	10	—	Horn-20|13°	TR Sep: 10 to 50 cm; Cyclic prefix length: 0, 4, 16 samples; Modulation order: BPSK, QPSK, 16 and 64-QAM	Develops attenuation model and tunes OFDM parameters to capture and counter frequency dependent hardware impairment.
	[36], [59]	120 – 140; 210 – 240; 1000 – 1050	2 to 32	∼ 60	Horn-25 – 40|10°	TR Sep: upto 40 cm; Modulation order: 16, 32 and 64-PSK, BPSK, QPSK, 16-QAM	Demonstrates and elaborates on the functioning of an experimental testbed consisting of analog frontend and digital signal processing backend.

Note: Ref-Reference, TR sep-Tx-Rx separation, AOI-Angle of incidence, AOR-Angle of reflection, HPBW-Half Power Beamwidth, Ant - Antenna, Type - Gain|HPBW: values of Tx/Rx for each attribute, same value for Tx and Rx if '/' missing.

[115], [117], [119], [120], [121], [122], [126], [136], [137], desktops [36], [59], [109], [112], [113], [114], [116], [117], [118], [123], [124], [125], conference rooms [33], [76], [115], [119], [121], data centers [74], [128], [129], [130], and in some not-so-common spaces like factory buildings [73], shopping malls [108], [111], and airport check-in halls [111], lecture rooms [127], to name a few using different channel sounders. Some dynamic channel characterization for UMi [80], [81], [82], [83], [84] and different railway communication channels [88], [89], [90], [138] have also been investigated using a TDC-based sounder and in an urban environment using a VNA-based sounder [55], [133], [134], [135]. The weather is predicted to have a huge influence on the THz links due to significant molecular absorption at certain frequencies in the spectrum window of interest and has been investigated in a controlled environment in [93], [124].

As can be observed from the summaries in Table 3-6 the THz channel measurement systems have predominantly been built in the 140 GHz, 220 GHz, and 300 GHz frequency bands, based on VNA, TDC, TDS, and other sounders. Even amongst these bands most of the current THz channel measurements focus on the below-300-GHz band especially in common scenarios like office rooms, and conference rooms while extensive channel measurements above 300 GHz are still missing from the literature. In the outdoor scenario, the situation is further skewed toward the initial two bands and there is a dire need for substantial measurement campaigns in the beyond 300 GHz band to characterize and understand the channel propagation. Although there have been some campaigns to study the characteristics of the MIMO channel across various THz bands there is a need for more extensive campaigns to gain further insight into the complicacies of MIMO THz channels. In conclusion, the behavior of THz band links is heavily scenario and application-dependent. To cite an instance, the challenges and requirements of deploying a network with wider coverage differ from that of a highly mobile network or one that prioritizes high data speed even if they use the same frequency band. When the problem has to be assessed across the different THz bands it becomes even more profound. Thus, to properly assess the potential and limitations of THz communications across different bands with large swathes of BW, it is indispensable to properly characterize the different aspects of the channel, which can only be obtained through extensive and relevant measurements.

IV. CHANNEL MODELING IN THZ BAND

A THz channel has disparate properties from the relatively well-studied cmWave [11] and mmWave channels [139], [140], [141], [142] which makes studying and modeling such a channel, a unique proposition. Some of the unique features of a THz channel that augments the challenge can be enumerated as

- As opposed to other bands for communication, in the THz band significant power is present not only in the LoS path but also in reflected paths (up to double bounce), scattered and diffracted paths, and hence it would not be prudent to simply ignore them while modeling the channel [143]. Furthermore, to obtain an insightful understanding, the channel needs to be studied under different spatiotemporal channel conditions [82].
- A comparison of the effect of using a single antenna with directional scanning to antenna arrays with beam steering on wave propagation needs fresh investigation for the THz band. In the said band, double-directional

channel measurement would be the obvious choice independent of the antenna structure. However, signal propagation using a single antenna with directional scanning has to be studied in a different light from the antenna array which can either involve a sparse antenna array with physical separation [144] or a densely packed antenna array in small form-factor giving rise to UM-MIMO [29]. Both the array structures address the distance limitation issue but while the former suffers from a large form factor making it suitable for only base station-like fixed structures the latter suffers from increased complexity.

- The various channel parameters such as path loss, angular and delay spread, and the broadening effects have to be accurately modeled and parameterized from the investigations which are affected by multiple factors such as operating frequency [72], propagation environment [2], and properties of the materials [61], [66] in the environment under investigation.

The channel modeling approaches as evidenced in literature can be broadly classified into -

- **Deterministic** [145]: It is site-specific and heavily relies on solving Maxwell's equation in a given scenario. Highly accurate results are obtained using this technique but it is computationally intensive.
- **Statistical, or stochastic** [146]: It is not exactly site-specific but describes mostly the type of environment (such as indoor, outdoor, indoor hotspot, etc.) and creates the model based on measurement data. The trade-off in this method compared to the former is in accuracy to complexity.
- **Hybrid** [147]: It marries the best of both deterministic and stochastic modeling approaches balancing the complexity and accuracy while negating most of their shortcomings.

In recent times, there has been some interest in modeling channels using the concepts of neural networks [148], [149], [150], [151], generative adversarial network (GAN) [152], [153], [154] and generative neural network (GNN) [155], [156]. However, all the referred works are in mmWave, and to the best of our knowledge using such an approach for THz channel, modeling is yet to be explored. In the rest of the section, we elaborate on the various efforts to model the THz band channels using the broadly classified aforementioned techniques. A comparison of the different modeling approaches in light of complexity, accuracy, and requirement of resources, information of site geometry, and materials are summarized in Table 7.

A. DETERMINISTIC MODELING

Deterministic channel models have a physical basis [157] and require a vivid description of the geometry of the environment such as terrain profile, location, and characteristics of reflector/scatterers like buildings, trees, etc for an outdoor environment or placement of tables, chairs, etc for a common indoor environment as well as orientation and deployment of Tx and Rx [158]. The model is completely dependent on the site of interest however they do not depend on extensive measurement data and can provide a very accurate prediction of signal propagation [157] at the cost of computational complexity. Deterministic modeling in general can be classified into the RT method [42], [145], [158], [159], [160], [161], [162], finite difference time domain (FDTD) method [163], [164], [165], [166], [167], [168] and method of moment (MoM) [169], [170]. The rest of the subsection elaborates on the application of the methods in modeling THz channels.

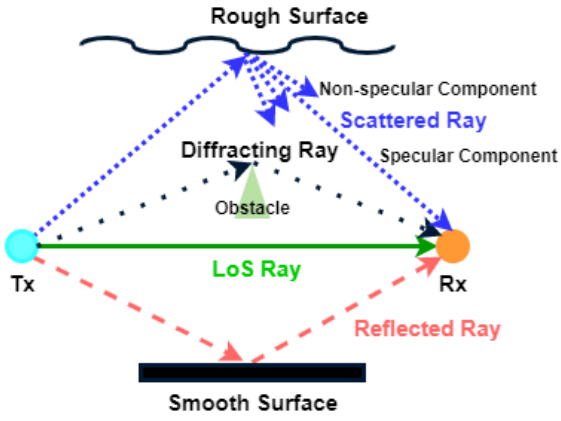

FIGURE 8. Typical RT modeling for THz band propagation.

1) RAY TRACING

Ray Tracing can be used with reasonable precision to predict the signal propagation in large buildings with numerous walls between Tx and Rx [157]. An RT model is based on the concept of approximating Maxwell's equation for electromagnetic wave propagation and geometrical optics. It uses the theory of geometric optic (GO), the geometric theory of diffraction (GTD), the uniform theory of diffraction (UTD), and Kirchoff Theory [171] to account for reflection of the propagating signal from smooth surface and diffraction from rectilinear surface [172].

During transmission, a signal encounters several objects in its propagation path giving rise to reflected, scattered, and diffracted copies of the LoS component as shown in Fig. 8 which needs to be traced adequately to accurately model the channel. A smooth surface only produces a reflected component whereas rough surfaces give rise to specular reflected components and non-specular scattered components. The specular component is dominant in the THz band whereas the non-specular components contribute significantly with an increase in frequency to the diffusely scattered power [52]. The classification of a surface as rough or smooth is dependent on the wavelength of the signal that is being propagated. If the wavelength of the propagating signal is comparable to or less than the standard deviation of the height of the

TABLE 7. Comparison of the different modeling approaches.

Methodologies	Deterministic	Statistical	Hybrid
Accuracy	High to Very high	Low	Medium to High
Complexity	High to Very high	Low	Medium to High
Resource Requirement	Extremely high	Low	Reasonable
Geometrical Information	Required in details	Minimally required	Required
Material Property	Preferably required in details	Minimally Required	Required

surface under consideration then the surface is treated as rough. Since the wavelength of signal in the THz band is low, common indoor surfaces such as plaster, and wallpaper appear as rough [50], [142] producing significant scattering which needs to be accounted for while modeling. On the other hand, the correlation length of a rough surface is much higher compared to the wavelength of a THz signal. Hence the appearance of sharp surface irregularities is minimal and the effect of diffraction is negligible in RT [126], [145]. Multi-ray propagation due to reflection, diffraction, and scattering are dependent on the angle, frequency, distance, and polarization in the THz band. While modified versions of the popular Kirchoff model [50], [52], [171], DS, and RCS [66] are used to characterize the interaction loss and model the reflected and scattered rays validating the measurement results, UTD [173] and Knife Edged Diffraction (KED) theory [117] are used to model diffraction in good agreement with measurement data. The major approaches for effectively implementing RT modeling are as follows

- **Visibility Tree** [174]: It generates a multi-layered tree-like structure as shown in Fig. 9b in order to effectively capture all the different rays in a propagation environment. At the outset, a fixed number of iterations $N_{\max}$ are fixed to limit the number of maximum reflections that are acceptable. For the representative scenario as shown in Fig. 9a $N_{\max}$ is fixed at 2 and hence a maximum of double bounce propagation is considered. As evident from Fig. 9b the Tx acts as the *root* of the tree and each of the branches in the layered structure represents the LoS link between the nodes (wedge, wall, Tx, Rx) in that particular layer. When the Rx is reached the link ends in a *leaf*. Once all the originated branches have concluded in a leaf it is just a matter of retracing each path from the leaf to the root in order to account for all the propagating rays in the considered scenario where the number of leaves represents the total number of paths identified by the method. The creation of the visibility tree however can be computationally intense.
- **Ray Launching** [159], [160], [172], [175], [176]: In this method, the rays are launched along all possible angles of azimuth (for 2D) or all possible combinations of azimuth and elevation angle (for 3D). The paths suffer a change in direction due to reflection, diffraction, etc, and are followed till the ray exits a predefined area of interest or becomes weaker than the assumed threshold, or reaches the destination. The method is more suited for the *canyon model* where the transmitter and receiver height is much smaller than the surrounding buildings and in scenarios where several receivers are serviced by a single Tx as in a cellular environment. However, diffraction in general and single Tx-Rx location pairs are time-intensive to model using this approach.
- **Image Method** [157], [177], [178], [179], [180]: In this method images of a source at all planes are generated. The images serve as secondary sources such that if we consider a total of N planes in a scenario, then after the first reflection there will be N images of a source, $N(N-1)$ images after the second reflection, $N(N-1)^2$ and so on. The visibility of the image sources at the destination depends on whether any reflected ray originates from it. Once a ray has reached the destination the attenuation associated with all the reflection terms is calculated. This method is suited for simple environments only.
- **Virtual Point Approximation** [181], [182]: In the case of a multi-antenna system, the employment of conventional RT models to characterize each Tx-Rx link can become unrealistically complex and expensive. To ease the computational burden in a complex multi-antenna system the concept of the virtual point was introduced as shown in Fig. 10. A single RT simulation is performed between the virtual points and the different parameters are extracted from it. The extracted parameters in conjunction with the array characteristics provide the nature of the channel between each Tx-Rx pair in the array. The idea is based on the concept that when the virtual point is located very close to the actual antennas it will see a very similar set of rays. The mapping process is performed by extrapolating the endpoints of each ray to the actual position of the elements after performing a LoS check and an electromagnetic calculation.
- **Point Cloud Ray Tracing** [183], [184], [185], [186], [187]: To improve the accuracy of the RT-based method laser scanning of the environment can provide point cloud data of the environment with higher precision. The data set can then be used for RT simulation with better precision at the cost of higher processing time. In [111], [188], [189] point cloud RT has been effectively used to model THz band channels in both indoor and outdoor scenarios.

There is no dearth in the usage of the RT method for modeling THz band channels. In [126] the authors used an advanced frequency domain RT approach to characterize an indoor

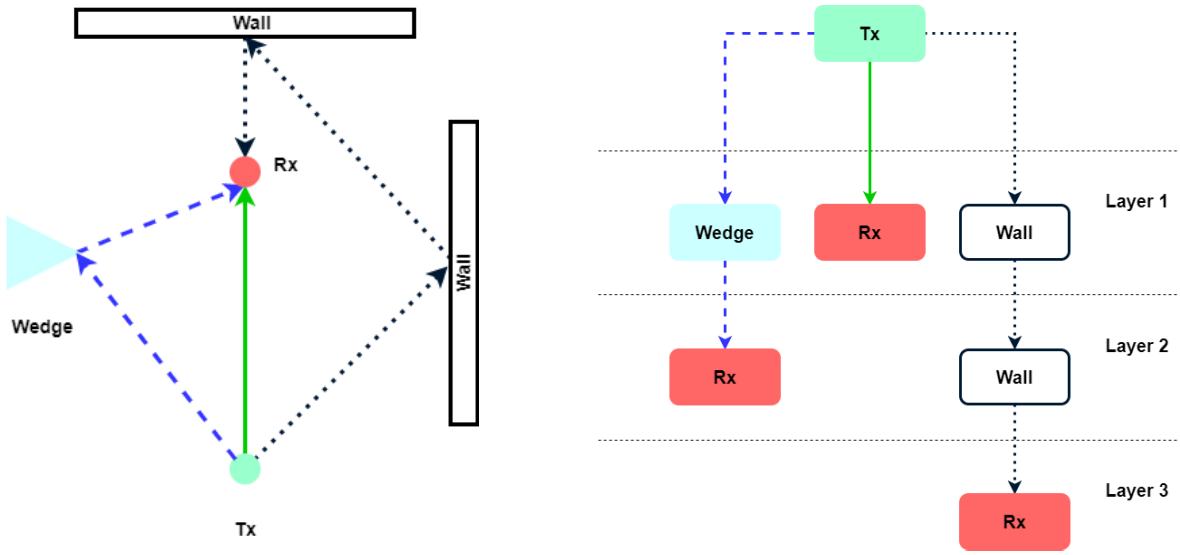

(a) Arbitrary propagation scenario

(b) Corresponding Visibility Tree representation

FIGURE 9. Illustration of visibility Tree representation.

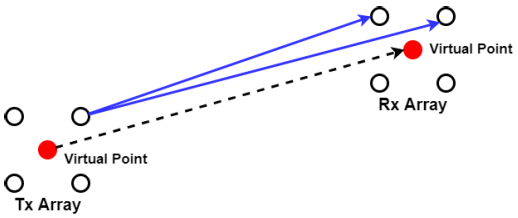

FIGURE 10. Virtual point approximation approach.

propagation channel which was validated and calibrated by the measurement data. A series of campaigns in relation to smart rail mobility utilized a measurement-validated and calibrated RT simulator to characterize InW [77], [78], T2T [89], T2I [88], infrastructure-to-infrastructure (I2I) in the perspective of railways and inside station [90] scenarios at 300 GHz. In [190] a novel 3D RT algorithm (RTA) based on the Beckmann-Kirchoff model was used for modeling non-specular components of diffused scattering whereas in [191] it was used to study the impact of diffuse scattering from regular elements in an office environment for MIMO channels at 300 and 350 GHz. A 3D THz channel model based on the RT technique was developed that includes graphene-based reflect antenna array response and 3D multipath propagation in [192] whereas in [145] a multi-ray channel model in the THz band was developed using ray tracing technique and the developed channel model was further analyzed to extract the channel parameters.

2) FINITE DIFFERENCE TIME DOMAIN

Based on GO, UTD, GTD, and similar concepts, RT produces a comparatively simple solution to radio propagation in scenarios containing large objects with well-defined sharp edges. However, most practical scenarios involve structures with complex material properties. In such situations, it is not possible to obtain any asymptotic solution but to numerically solve Maxwell's equation. FDTD is one such method that produces a pretty accurate result by taking into consideration the effect of each object in a given environment.

However, FDTD is not without its fair share of limitations. The main disadvantage of FDTD is the requirement of vast swathes of memory to store the solutions at each location and support extensive calculations to update the solutions at each time instant. Depending on the area under test such intensive computation might be overkill in certain regions while in others it might not be feasible to support such intense numerical analysis due to the computational resources required. In order to address the said problem, a hybrid technique based on a combination of RT and FDTD was proposed in [165] which is further elaborated in subsection IV-C.

FDTD had been effectively used for modeling ultra-wideband indoor propagation by subdividing an 8 GHz wide channel into 8 sub-channels and then applying FDTD to characterize the CIR for each of the sub-channels in [168]. A multi-mode FDTD approach that takes into account the antenna properties had been used in [164] to characterize an indoor propagation environment. The indoor channel for a residence was characterized at the 900 MHz Industrial, Scientific, Medical (ISM) band using reduced FDTD which is a memory-efficient version of the general FDTD approach.

In the THz domain, the FDTD approach had been mostly used to study the wave propagation through various forms of plasma such as unmagnetized plasma slab [193], dusty plasma [194] and time-varying plasma [195] to name a few. Investigation of wave propagation through multi-layer

medium structure using FDTD for THz imaging application had been conducted in [196]. In [197], the intra-device electromagnetic wave propagation was studied in THz frequencies using FDTD, and the performance was compared to the results obtained using RT.

3) METHOD OF MOMENT

As evidenced and explained earlier RT works well when modeling a large environment containing big objects but in scenarios with smaller obstacles, reflectors, etc requiring higher precision and complex analysis the method encounters its limitation and a better alternative is the MoM. A combination of the methods can also be used to good effect where either the accuracy of modeling can be improved [198], [199] or for using the optimized method based as a trade-off between accuracy and computational complexity [169], [170]. The solutions determined by the MoM for objects which are of a size comparable to the transmitted signal wavelength are numerically superior compared to other approaches, especially RT but that comes at a cost of higher computational time and larger memory space.

In [200], the MoM method was used to analyze the electromagnetic shielding and scattering properties of 2D materials composed of metal, dielectric or magnetic material in the presence of a lossy half space which simulates the effects of earth ground. The solution of this method was compared to that obtained using the RT method for evaluating the wave propagation and penetration properties in an indoor wireless environment at 150 and 450 MHz in [169]. The transmission of ultra-high frequency (UHF) signal through a windowed wall was studied using a combination of solutions to bound integral and MoM in [170]. A hybrid approach was used as mentioned earlier in [198] and [199]. In [198] RT was used to characterize an indoor scenario at 900 MHz by considering direct, reflected, and transmitted paths, wave polarization, and antenna pattern. In the event where accuracy constraint was not met the more complex MoM method was used to provide a better model. While in [199], the MoM was used to extract the specular and grating transmission and reflection coefficient of periodic structures present in the studied indoor environment. The obtained data were then fed as input to an RT program to obtain the effect at the receiving antenna and characterize the propagation environment. The usage of MoM for modeling THz channel links has not yet been studied so far to the best of our knowledge.

B. STATISTICAL MODELING

Although deterministic models are known to provide accurate models of the given scenario, they are extremely site-specific and computationally complex. They often require huge volumes of memory space to update information. In contrast statistical model although at times bear similarity to deterministic models are not site-specific but are rather specific to the type of environment (rural, urban, microcell, etc), does not require detailed geometry of the environment being modeled, and are computationally tractable. Due to these prior advantages, statistical modeling is favored since it facilitates fast-channel model construction. Statistical modeling can be classified either on the basis of information available for modeling or on the basis of information that is obtained as a result of the modeling. The former classifies statistical modeling as GBSM and nongeometrical stochastic channel model (NGSM) while the latter classifies it as an analytical and physical model.

Due to large swathes of BW available at THz frequency any developed channel model needs to account for the possibility of having several resolvable MPCs and cannot be modeled by using Rayleigh or Rician fading as is done for lower frequencies. In that respect, THz band channels can be loosely compared to ultrawideband (UWB) channels where various propagation parameters are frequency or distance-dependent, or both. In addition, delay and angular dispersion have a significant impact on the propagating wave and narrowband path loss models are no longer valid [201]. Similar modifications and even more need to be done for modeling a THz propagation channel. A statistical impulse response model needs to be developed for the THz band where the multipath parameters are defined by statistical distributions [143]. In this regard, a novel stochastic 300 GHz indoor channel model is introduced in [146] by combining both time and frequency domain modeling to account for frequency dispersion at the said frequency. In addition, to model MIMO as well as other novel antenna systems amplitude, phase, spatial, and temporal channel information are considered for the modeling process. The generated model is compared with results obtained from measurement calibrated and validated RT simulator for an indoor office scenario and is found to be in good agreement.

1) GBSM VS NGSM

GBSM as the name suggests depends on the geometry of the site being modeled. Thus it is the statistical modeling concept that bears similarity with deterministic models which require detailed geometry of the site being modeled. The difference between the two however augurs from the fact that in deterministic the location of the scatterers has to be precisely defined to get an accurate model whereas in GBSM the scatterer locations are stochastically obtained as per certain distributions [202]. The idea of geometry stochastic modeling was introduced for a mobile radio system in [203], [204], [205], and a macrocell mobile environment in [206]. Post the stochastic placement of scatterers the wave propagation is analyzed by tracking the reflected, diffracted, and scattered rays like in RT simulations except now only a subset of the available rays is considered for modeling to make the problem tractable. In [203] a configurable statistical channel model using multi-directive antennas is presented. The developed model is used to simulate a code division multiple access (CDMA) channel with multiple directive antennas and joint detection. The model developed in [206] can provide the

statistics of the AOA which is crucial to understanding the effect of a directive antenna at the base station. The model considers upto single bounce reflected rays and assumes the placement of the scatterers uniformly on a circle around the mobile. A similar antenna array at the base station is considered while modeling the diffuse scattering in the presence of dense discrete scatterers in [204]. An algebraic power decay is used for the path loss and the model is compared with measurement results at 1800 MHz to explain the phenomenon of diffuse background scattering in a rural and urban environment. A unified mobile channel model is generated in [205] by using the information on the time evolution of scattering processes and directions of arrival. At THz band in indoor scenarios, a reference regular-shaped GBSM (RS-GBSM) is proposed in [207] as a combination of the two-sphere model and cylindrical elliptical model by considering LoS, single bounce, and double bounce components at the receiver. The von Mises-Fisher (VMF) distribution, used in conjunction with the azimuth and the elevation angle gives the scatterer distribution. A non-stationary GBSM for THz communication systems utilizing UM-MIMO for long traveling distances and assuming frequency-dependent diffuse scattering is proposed in [208].

In comparison NGSM also known as parametric stochastic models (PSM) is a purely stochastic process [27] and has no dependence on the geometry of the type of environment being modeled. NGSMs are known for their simpler structures and lower computational burden compared to GBSMs. However, they suffer while capturing the effects of complex phenomenons such as frequency, time, and distance dependence of channel parameters as well as channel variation due to the movement of mobile elements in an environment which is common in THz band channels. NGSMs define the channel parameters based on some underlying probability distribution function and are independent of the propagation environment being modeled. They characterize the statistics of the channel measurements instead of their actual values using measurement data or those generated using RT. An NGSM model based on physical wave propagation through a channel characterized by its MPCs, AOA, and AOD [209], delay and loss [210] is present in literature. Relating the AOA and AOD to the LoS gives a unique advantage to the model where it becomes independent of the site geometry. The appearance and disappearance of the MPCs are modeled by a genetic process where changing the delay time of the propagating path can efficiently capture the Doppler properties of the channel. The model is based on data generated by a calibrated and validated RT tool which is tuned for narrowband, wideband, and directional channel measurement. While the model in [209] can simulate any complex system with arbitrary antenna configuration and pattern, it was tuned further in [210] to cater to the specific requirements of advanced communication systems with multiple antennas. An analysis of the MPC parameter estimation accuracy was conducted in [211] where a Gaussian antenna beam pattern was considered.

2) ANALYTICAL VS PHYSICAL

The physical channel model provides the statistics of the channel characteristics which are not dependent on the antenna pattern such as power delay profile, arrival time, etc. while the analytical model characterizes the CIR including the antenna characteristics [212], [213].

In a multi-antenna scenario that is of special interest in the THz band due to its directive properties, the analytical model arranges the individual CIRs between elements of the multi-antenna system in a matrix and then describes their statistical properties including the correlation between them. This is known as the *matrix-based model*. In a simplified model, the channel between each element is assumed to be an independent and identically distributed complex Gaussian channel with approximately uncorrelated antenna characteristics such that the fading process can be modeled as a simple Rayleigh process. However, such simplicity does not make sense at the THz band due to the sparsity in the space domain. In the Kronecker model [214], the correlation between individual channels is assumed but for simplification, it is assumed that the antenna responses at the Tx and Rx are separable. But, in the THz band with an increase in the number of antennas in an array to support UM-MIMO or a decrease in communication distance due to a small LoS path such an assumption becomes less valid [215]. In addition, for a UM-MIMO configuration, the antenna structure can no longer be considered a point source; hence, the far-field assumption also becomes invalid [216].

To overcome the prior mentioned shortcoming, virtual channel representation (VCR) characterizes the channel by sampling rays in a beam space [217], [218], [219]. A fully correlated channel matrix is used to provide a beam domain channel model that can be applied to a wide variety of propagation environments. But the concept is applicable to only uniform linear array structures. A combination of the Kronecker model and VCR was presented in [220]. It is a more generic framework that is applicable to any type of array structure and also considers the joint spatial correlation of Tx and Rx as opposed to the Kronecker model. The aforementioned models are favored for massive MIMO because of their low complexity but are not suited for THz links due to their presumptions on the far-field effect and stationarity of the channel. To adapt them for THz channels a beam domain channel model with no far-field assumption was presented in [219] and in [213] where the spherical wavefront and space-time non-stationarity was considered in addition. An analytical model based on space-time coding has generated renewed interest in light of the 6G wireless network implementation which is anticipated to provide ubiquitous connectivity [221]. Other analytical models include the diagonal-decorrelation model where the cross-correlation across antennas is assumed to be zero [222], the rough surface model for theoretically computing the spatial correlation relative to scattering surface profile [223] which could be utilized for modeling scatterer rich THz channels and structured model [224] which is an

extended version of the model in [220] based on tensor calculus.

The GBSM models discussed in subsubsection IV-B1 also fall under the purview of physical models. Physical models also include the one-ring model, the combined elliptical model, and the one-disk model which are recognized under the umbrella head - *geometry-based statistical propagation models*. The one-ring model is the most popular GBSM applicable to MIMO channels [216], [225], [226] which accounts for local dispersion from obstacles placed on a ring around a subscriber unit. This model might not always be in agreement with the Kronecker model as shown in [216]. The combined elliptical ring model is characterized by a parameter known as the local scattering ratio (LSR) which is an indication of the omnidirectional distribution of scatterer on a local ring and a low value represents directional scatterer distribution [225], [227]. The one-disk model on the other hand comprises a single large disk between the Tx and Rx where the scatterers are evenly spaced [228]. The correlation properties of the model are dependent on the path loss exponent and are known to have low antenna correlation while the magnitude cross-correlation is high.

A geometry-based statistical channel model for THz band propagation was proposed in [229] which can not only provide physical characteristics but can also investigate system-level performance. In [230] Saleh and Valenzuela based on the pioneering work of [231] introduced the concept of clustering related to MPCs for the first time which popularly came to be known as the S-V model. In addition, they modeled the inter and intra-cluster arrival time as a Poisson process and the received power as an exponentially decaying function of delay. However, the model was built based on measurements conducted using omnidirectional antennas and hence omits AOA and AOD characterization. In the THz domain, it is important to incorporate such characterization due to its highly directive nature which requires the specification of direction of arrival (DOA) and direction of departure (DOD). In [96], [229] a spatially extended S-V model was introduced which approximated DOA/DOD distribution as a zero-mean second-order gaussian mixture model (GMM). In some other research works, the arrival time is modeled differently from a Poisson process to have better agreement with measurement data [146], [232], [233], [234]. Similar modifications to the S-V model are introduced in some early channel modeling done for mmWave and THz channels [235], [236], [237] to match with the calibration and validation process.

C. HYBRID MODELING

Given the huge variation in propagation environment for various applications, it is prudent to move away from a stringent approach based on a particular concept and use a more amenable hybrid approach based on marrying the best of different concepts and thereby possibly addressing the majority of their shortcomings. The deterministic approaches for example are known for their accuracy but suffer from complexity and high time consumption. The statistical approaches on the other hand are preferred for their simplicity but suffer from lowered accuracy. Even amongst different deterministic or stochastic approaches, there are variations in their benefits and limitations. To address such challenges and provide an optimum solution different hybrid approaches combining various deterministic approaches [165], [238], [239] or deterministic and stochastic approaches [96], [240], [241], [242], [243], [244], [245] are proposed. The details of such trade-offs are further elaborated in subsubsections IV-C1 and IV-C2.

1) DETERMINISTIC HYBRID APPROACH

The FDTD approach is known to provide very accurate modeling of channels consisting of complex structures and boundary discontinuities but it comes at a higher computational cost. The RT approach on the other hand requires comparatively fewer computational resources for modeling the above-mentioned scenarios but is not as accurate. In a typical site, rarely would we come across scenarios that consist of only complex structures or boundary discontinuities so as to invoke the resource-intensive FDTD method every time. A more practical scenario might be the one shown in Fig. 11 consisting of a mixture of complex and simple structures where the complex structures can be modeled using FDTD while the rest of the scenario is modeled using the comparatively simpler RT approach. As we go up in frequency, the otherwise smooth-looking surfaces tend to appear rough due to the comparable wavelength of the transmitted signal. Thus, in the THz band, the FDTD method can resolve small and complex scatterers and rough surfaces [2] while geometrical optics-based RT can be used for modeling the rest of the environment providing an optimal trade-off between accuracy and complexity.

The combined technique using RT and FDTD to model an indoor propagation environment and penetration of waves from outdoor to indoor (O2I) at 2.4 GHz was presented in [165]. As explained earlier the hybrid approach was used to good effect to model the small complex discontinuities using FDTD and the wide area using the RT approach. The numerical results from the model were found to be in sync with the known exact solutions as well as measurement data for the outside-to-inside penetrating wave. The model was found to be a generic one and could be suitably adapted to other frequencies after suitable adjustments. In [238], UTD was used to model objects much greater than the wavelength of the transmitting wave whereas the complex and small scattering objects were modeled using FDTD in the context of the Wi-Fi transmission system where the model was used to evaluate the bit error rate (BER). A three-dimensional deterministic hybrid approach combining time domain parabolic equation (TDPE) with FDTD was proposed in [246] for O2I radio wave propagation. A limitation of the deterministic hybrid approach however is the smooth transition between FDTD

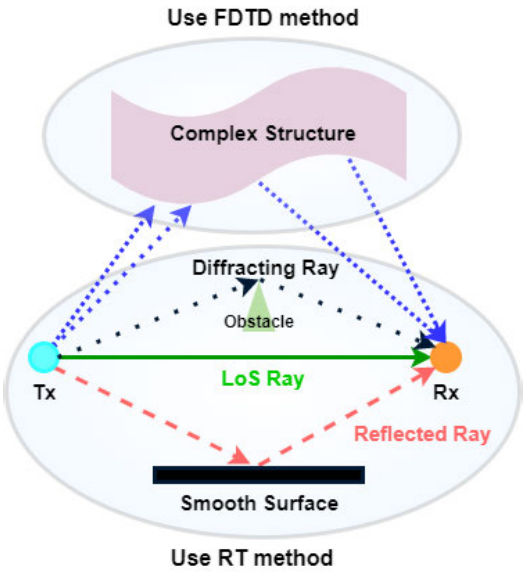

FIGURE 11. A representative scenario to model using RT-FDTD hybrid approach.

and the other method that is being used if there are too many boundaries in a given scenario.

2) STOCHASTIC-DETERMINISTIC HYBRID APPROACH

If accuracy is not a concern then the simplest way to model a given scenario is by using the statistical approach. However, as the statistical approaches do not capture the detailed geometry of the measurement environment they are not able to consistently reproduce the scenario and hence capture the effect of the movement of mobile stations in the environment. Similarly, the effect of change in direction and angle of transmission or reception due to the dynamic nature of the site is also not defined. In addition, in a multi-antenna communication system, which is supposed to be very common for the THz band due to its inherent directional properties, the correlation between the links is not captured since the random generation of propagation links cannot guarantee the same effect every time. Thus a hybrid solution using the geometrical approach to compensate for the limitations of the stochastic approach can provide the important missing features to a generated channel model [139], [241], [242], [243], [244], [247], [248], [249].

The quasi-deterministic (Q-D) model is a popular hybrid approach that is generated by first obtaining the dominant MPCs from environment geometry and then simulating a cluster of MPCs associated with the dominant MPCs. The intra-cluster MPCs are therefore expected to have similar DOA, DOD, and delay with a small spread being very close to one another. In addition, to characterize the scatterers and capture the dynamic nature of the environment additional MPCs are considered. The Q-D channel model has been successfully applied and validated for different applications such as cmWave propagation [240], [250], indoor mmWave propagation [141], [142], [251], indoor sub-THz propagation [96], [121], [229], mmWave Evolution for Backhaul and Access (MiWEBA) [242], [244] and IEEE 802.11ay [252]. In [240], the geometry and routing path of mobile stations were first identified in a *virtual cell deployment area (VCDA)*, following which the delays and DOAs were traced by geometrical means. The intra-cluster parameters such as delay, angular dispersion, and average power of multipath components were stochastically modeled. The model was specifically created for European urban microcells with the possibility to adapt to similar regions in American or Asian cities. In [250], on the other hand, the hybrid model was designed for indoor environments which used a stochastic approach for modeling the dense MPCs and a Q-D approach for modeling the dominant MPCs to capture the spatial behavior. In [142], the propagation channel of a conference room at 60 GHz was characterized by a hybrid model, and various inter-cluster, intra-cluster, and polarization parameters were statistically defined using experimental results and RT simulations. Q-D models were also developed and parameterized for 60 GHz signal propagation for open square [242], non-stationary environment [244], various office environment [141] and in corridor [139]. In all the scenarios, the dominant paths (only two were considered - LoS and ground reflected paths) were considered deterministically whereas the comparatively weaker random reflected rays were modeled stochastically where cluster arrival was modeled as a Poisson process and inter-arrival time as exponentially distributed. In [121], on the other hand for THz communication in an indoor environment, both the inter-cluster and intra-cluster arrival time was modeled as a Poisson process and Von Mises distribution was used for generating AOA of both inter and intra-cluster subpaths.

V. OPEN CHALLENGES AND FUTURE SCOPE IN THZ BAND

Despite an avid interest and best effort to study the distinctive attributes of a THz band channel, there still remain several challenges that need addressing. In this current section, we look at some of those challenges from the perspective of channel sounding, measurement campaigns, and modeling in the band of interest.

A. CHALLENGES IN CHANNEL SOUNDING

The THz band due to its distinctive attributes has requirements that were never a major concern while building a channel sounder to study the lower frequency channels. Some of the unique requirements and the challenges they present can be enlisted as

- Requirement of the high carrier frequency to the tune of THz is required to study the channel which in turn boils down to the requirement of suitable hardware that can generate such high frequencies with adequate stability. In VNA-based sounding 4-port VNAs are preferred over

the traditional 2-port ones to increase the VNA stock frequency range to the frequency of interest through heterodyning [62], [253]. However, the usage of extra hardware not only incorporates additional losses which subsequently reduces the dynamic range-one of the major requirements as mentioned later but also limits the possibility of conducting campaigns in dynamic vehicular, railway, and other such scenarios where the Tx or Rx or both are in motion. Thus there is a need to develop and design compact, portable sounders with minimal hardware footprint. Sounders in reasonable form factors would also have reduced power requirements further supplementing the ease of mobile measurement.

- Next is the requirement for directional antennas and solely so as opposed to a combination of omnidirectional and directional ones that were used even for studying the quasi-directional mmWave signal propagation.
- The systems also need to support fast channel acquisition to appropriately capture the channel variability inherently characterized by short coherence time which is not possible with the widely used directional scanning approach. In this context, the challenge lies in the development of low-cost commercial phased arrays that can support fast beam sweeping to capture the directional attributes of THz band propagation in real time. Commercial adaptation of experimental solutions proposed in [254], [255], [256] can possibly accelerate the process. Another experimental demonstration in [257] consists of transceiver arrays with 8 parallel channels at 140 GHz that can be used either in digital MIMO configuration or in hybrid beamforming architecture in conjunction with an analog antenna array.
- Capability to handle large BW of the order of several GHz or maybe even THz. Such large BW creates a smaller delay resolution which should be captured to identify a more precise propagation path. In addition, due to the large carrier frequency, the effect of Doppler is expected to be more stringent compared to lower frequencies. Furthermore, the imprecise operation of a clock can lead to an artificial Doppler shift. Thus the challenge lies in designing highly precise clocks and inexpensive and energy-efficient ADCs that can meet the stringent requirements of synchronization and high sampling rate.
- Due to high transmission rates at the THz band, sampling and sophisticated processing of the received signal become quite complicated. This calls for innovation in synchronization techniques. In the context of transmission using pulse-based modulation some novel techniques using iterative observation window shortening [258] and jointly initiated handshake mechanism [259] have been proposed. However innovative techniques for carrier-based scenarios and MIMO systems customized to the unique features of THz band communication needs further exploration. Furthermore, a comprehensive mechanism that not only provides timing synchronization but also frequency and phase synchronization needs to be investigated.
- Higher dynamic range and sensitivity to identify more significant MPCs in the face of massive path loss. Although new algorithms are developed to improve the noise floor estimation and further noise removal during post-processing [260], [261] more needs to be done to further improve the dynamic range and sensitivity of measurement systems since the transmitting power of the current THz band systems is quite limited to facilitate long-distance measurement campaign.
- Measurement distance scalability is another requirement and subsequent challenges that are associated with it need addressing. As can be observed from section III majority of the measurements are done using systems built with VNA which are known to provide limited separation between transmitter and receiver. Such a limitation has been improved by the usage of the RFoF concept [55] which can support a separation of upto 100 m but then suffers from the slow speed of acquiring channel response. The TDC-based approach can support measurement distances of several meters but suffers from complex synchronization procedures for long-distance measurements as listed in Table. 2. In this context, a hybrid-sounding approach that reaps the benefit of implicit synchronization in a VNA-based sounding and yet facilitates fast channel acquisition might be worth investigating.

In a nutshell, a comprehensive high-performance measurement system, meeting the aforementioned generic requirements of a THz band channel and adapting itself to further site-specific requirements needs extensive research and investigation.

B. CHALLENGES AND FUTURE DIRECTIONS IN CHANNEL MEASUREMENT

The THz band is envisioned to be used for a plethora of applications beyond just wireless communication such as wireless cognition [262], [263], imaging [264], sensing [265] and precise positioning [264]. Even in wireless communication, there will be several applications in addition to mobile communication such as wireless fiber for backhaul [266], intra-device radio communication [267], and wireless links in data centers [21]. Such a varied palate of applications brings with it unique challenges and requirements that can be identified and addressed through extensive channel measurements conducted to investigate the feasibility of each of the implementations and are summarized as follows

- As is evident from the elaboration in section III most of the measurements in the band of interest have been in scenarios that are traditional like an indoor office environment, conference rooms, laboratory desktops, and rooms of different sizes. To facilitate the design of the physical layer mechanisms which adequately capture the frequency selectivity of ultra-wideband channels in

high data-rate indoor applications further targeted measurement campaigns are required in scenarios such as factory [73], stadium (open-roof), gymnasium (close-roof), auditoriums [268] to name a few.

- The number of outdoor measurement campaigns is very limited and needs to be earnestly considered since the dynamic behavior of a channel and its effect is more prominent in outdoor scenarios. The exploration of the behavior of THz band channels in dynamic scenarios is almost negligible for any scenarios - indoor, outdoor, or otherwise and needs to be studied for proper modeling of human body blocking, reflection, and scattering from apparently smooth, reflective mobile objects, and such phenomenon.
- The investigation of links for on-chip communications and in data centers still needs further deliberations to identify their distinctiveness and explore the feasibility of applications envisioned for nano-communications.
- Although there have been some measurement campaigns to study the THz band channel in the context of smart railway applications, the campaigns in the context of studying the vehicular channel are quite limited. Both scenarios require more extensive campaigns in different scenarios in the specified frequency band to support the design and development of standards that can realize the vision of autonomous intelligent transport. In addition, efforts need to be invested to conduct campaigns to study the unique attributes of scenarios such as unmanned aerial vehicle-assisted wireless communication, airplane-satellite communication, and satellite-to-satellite communication [2].
- In the measurement campaigns for the THz band, the frequencies that have been explored so far are mostly below 500 GHz which means there are large swathes of the spectrum that still need investigation.
- Integration of ground and airborne networks to support all-pervasive communication in 3D space is outlined for THz band communication. Realizing such advanced features, which are very different from conventional 2D networks would require extensive measurements to facilitate new approaches for 3D frequency and network planning involving communication between terrestrial base stations and tethered balloon or drone base stations [269].
- THz communication is envisioned to take a leap from massive MIMO to the usage of the intelligent reflective surface (IRS) which will also enable innovative ways of communication such as by using holographic radio frequency (HRF) and holographic MIMO (H-MIMO) [221]. In this context, campaigns need to be designed to identify the optimal placement of such passive reflective surfaces and conduct a fundamental analysis of their performance in enhancing communication range, coverage [270], spectral efficiency, and network capacity.

In conclusion, despite the best efforts by various research groups across the world, there are gaps that still need filling from the measurement perspective to realize the ambitious plans that have been drawn for THz band communication. Extensive measurements can pave the way for the creation of simulators that can effectively capture the peculiarities of THz frequencies and can generate a huge amount of measurement data that would be required for novel channel modeling approaches. The importance of huge measurement datasets is further substantiated in the next subsection.

C. CHALLENGES AND FUTURE DIRECTIONS IN CHANNEL MODELING

As for the other subsection heads, in the domain of modeling, as well THz band channels present unique challenges where diffraction is expected to have a lesser effect on signal propagation compared to lower frequencies while scattering is going to have a more predominant effect due to comparable wavelength of THz signals to the size of dust grains, raindrops, roughness on walls [102]. A lot of energy is invested by research groups across the world to accurately model a THz band channel with an optimal trade-off between accuracy and complexity. In this sphere, the challenges and requirements include but are not limited to the following

- A ray-tracing statistical hybrid model presents a reasonable solution that has been used for modeling various communication scenarios. However, to the best of our knowledge, an accurate channel model for NLoS which can capture the effects of diffuse scattering is missing.
- While it is easier to extract channel parameters from statistical models, the extraction of the same from a deterministic-statistical hybrid model is not as straightforward and requires a large amount of measurement data [121], [241], justifying our previous claim of further extensive measurement campaigns and investigation of the same.
- Artificial intelligence (AI) and machine learning (ML) techniques are known to be adept to solve complicated problems. Hence it can be expected that in the event of the availability of large measurement datasets (that can be generated by using measurement-validated simulators), the true potential of the techniques can be harnessed in clustering MPCs, extracting channel parameters, and developing novel learning-based channel models. AI-based approaches are already been used in mmWave channels, for path loss prediction [271], [272] and for clustering using unsupervised learning, [273]. Thus it would be feasible and possibly more suited to use such techniques for modeling and extraction of channel parameters for the more complex THz band. The implementation of the same needs to be explored.
- As explained earlier usage of UM-MIMO and IRS are realistic in a THz band communication setup due to

the possibility to build them in a small form factor and their ability to solve the issues related to LoS blockage and scattering problems. However, both technologies present new challenges to deal with, such as modeling of mutual coupling effect and near field effects [27]. The analysis of the mutual coupling effect tuned to THz transceivers is important to study the effect of the same on the performance of UM-MIMO and IRS. As for near-field effects, efforts are required to experimentally characterize the same since the THz band is visioned to support short-distance communications too which might be less than the Rayleigh distance. Simple assumptions as is done currently would lead to erroneous results in such scenarios.

- Even as ultra-wideband communication at the THz band promises improved channel capacity the frequency selectivity of such wideband channels needs to be considered to model joint propagation characteristics in multi-band operations, to investigate any correlation between bands, and to suggest an appropriate physical layer design. The temporal birth-death (BD) process of MPCs due to the temporal variability of scatterers either needs to be freshly modeled in the context of the THz band or validated for the existing models in mmWave and lower frequency bands. The spatial BD process in the context of UM-MIMO on the other hand is still completely unexplored and needs to be modeled afresh to analyze the impact.
- The current research on spatial consistency which is acknowledged by 3GPP as an important channel modeling component [268] is currently based on omnidirectional antennas at the Tx and Rx [274] and needs to be adapted to include the effect of directionality since THz band communication is proposed to be majorly based on the usage of directional antennas which has not been explored yet. In addition, polarization properties, azimuth, and elevation angles of departure and arrival of MPCs need to be suitably accounted for in the developed models [275].

To draw an inference as emphasized earlier, the THz band has its unique features and new techniques are being used to derive the best out of the band of frequencies. In that context, the channels should be modeled using innovative approaches with feasible complexity and computational demand and not be mere extensions of the existing models to the new frequency bands. Several works in that direction are already in progress but as emphasized earlier, more needs to be done to comprehensively capture all the uniqueness of the band.

VI. CONCLUSION

The current monograph sequentially presents an insightful and focused overview of channel sounding techniques, channel measurements, and channel modeling for THz communications followed by the identification of open issues in the context of the prior three topics. A total of four channel sounding techniques are comprehensively reviewed and their suitability for studying the THz band propagation is assessed including the less explored sounder comprising of a combination of a signal generator and analyzer. A novel in-house SGSA-based channel sounder is also briefly presented in this context. An exhaustive overview of the measurements across the band of frequencies for different indoor, outdoor, and other unique scenarios available in the literature is presented and summarized. The summary helps in identifying the gaps and subsequently the need for further extensive campaigns to characterize a THz band channel in a given scenario with improved confidence. The paper then presents a comparative study of the different modeling techniques available in the literature, their pros and cons, and their suitability to model THz communication channels. The challenges in using the existing channel models to characterize a THz band channel and the possible modifications required to capture their uniqueness are also disseminated. The study concludes that further effort is needed before a standard for THz channel sounding, measurement, and modeling is obtained.

REFERENCES

[1] I. F. Akyildiz, J. M. Jornet, and C. Han, "TeraNets: Ultra-broadband communication networks in the terahertz band," *IEEE Wireless Commun.*, vol. 21, no. 4, pp. 130–135, Aug. 2014.

[2] I. F. Akyildiz, C. Han, Z. Hu, S. Nie, and J. M. Jornet, "Terahertz band communication: An old problem revisited and research directions for the next decade," *IEEE Trans. Commun.*, vol. 70, no. 6, pp. 4250–4285, Jun. 2022.

[3] H. Kaushal and G. Kaddoum, "Optical communication in space: Challenges and mitigation techniques," *IEEE Commun. Surveys Tuts.*, vol. 19, no. 1, pp. 57–96, 1st Quart., 2017.

[4] D. Heatley, D. Wisely, I. Neild, and P. Cochrane, "Optical wireless: The story so far," *IEEE Commun. Mag.*, vol. 36, no. 12, pp. 72–74, Dec. 1998.

[5] C. X. Wang, J. Huang, H. Wang, X. Gao, X. You, and Y. Hao, "6G wireless channel measurements and models: Trends and challenges," *IEEE Veh. Technol. Mag.*, vol. 15, no. 4, pp. 22–32, Dec. 2020.

[6] H. Tataria, M. Shafi, A. F. Molisch, M. Dohler, H. Sjöland, and F. Tufvesson, "6G wireless systems: Vision, requirements, challenges, insights, and opportunities," *Proc. IEEE*, vol. 109, no. 7, pp. 1166–1199, Jul. 2021.

[7] M. Shafi, J. Zhang, H. Tataria, A. F. Molisch, S. Sun, T. S. Rappaport, F. Tufvesson, S. Wu, and K. Kitao, "Microwave vs. millimeter-wave propagation channels: Key differences and impact on 5G cellular systems," *IEEE Commun. Mag.*, vol. 56, no. 12, pp. 14–20, Dec. 2018.

[8] T. S. Rappaport, G. R. Maccartney, M. K. Samimi, and S. Sun, "Wideband millimeter-wave propagation measurements and channel models for future wireless communication system design," *IEEE Trans. Commun.*, vol. 63, no. 9, pp. 3029–3056, Sep. 2015.

[9] M. Xiao, S. Mumtaz, Y. Huang, L. Dai, Y. Li, M. Matthaiou, G. K. Karagiannidis, E. Bjornson, K. Yang, I. Chih-Lin, and A. Ghosh, "Millimeter wave communications for future mobile networks," *IEEE J. Sel. Areas Commun.*, vol. 35, no. 9, pp. 1909–1935, Sep. 2017.

[10] C.-X. Wang, J. Bian, J. Sun, W. Zhang, and M. Zhang, "A survey of 5G channel measurements and models," *IEEE Commun. Surveys Tuts.*, vol. 20, no. 4, pp. 3142–3168, 4th Quart., 2018.

[11] M. Kim, J.-I. Takada, and K. Saito, "Multi-dimensional radio channel measurement, analysis and modeling for high frequency bands," *IEICE Trans. Commun.*, vol. E101.B, no. 2, pp. 293–308, 2018.

[12] S. Salous, V. D. Esposti, F. Fuschini, R. S. Thomae, R. Mueller, D. Dupleich, K. Haneda, J.-M. M. Garcia-Pardo, J. P. Garcia, D. P. Gaillot, S. Hur, and M. Nekovee, "Millimeter-wave propagation: Characterization and modeling toward fifth-generation systems. [Wireless corner]," *IEEE Antennas Propag. Mag.*, vol. 58, no. 6, pp. 115–127, Dec. 2016.

[13] M. Shafi, A. F. Molisch, P. J. Smith, T. Haustein, P. Zhu, P. De Silva, F. Tufvesson, A. Benjebbour, and G. Wunder, "5G: A tutorial overview of standards, trials, challenges, deployment, and practice," *IEEE J. Sel. Areas Commun.*, vol. 35, no. 6, pp. 1201–1221, Jun. 2017.

[14] J. Huang, Y. Liu, C.-X. Wang, J. Sun, and H. Xiao, "5G millimeter wave channel sounders, measurements, and models: Recent developments and future challenges," *IEEE Commun. Mag.*, vol. 57, no. 1, pp. 138–145, Jan. 2019.

[15] T. S. Rappaport, K. A. Remley, C. Gentile, A. F. Molisch, and A. Zajic, *Radio Propagation Measurements and Channel Modeling: Best Practices for Millimeter-Wave and Sub-Terahertz Frequencies*. Cambridge, U.K.: Cambridge Univ. Press, 2022.

[16] H. H. H. Mahmoud, A. A. Amer, and T. Ismail, "6G: A comprehensive survey on technologies, applications, challenges, and research problems," *Trans. Emerg. Telecommun. Technol.*, vol. 32, no. 4, Apr. 2021, Art. no. e4233. [Online]. Available: https://onlinelibrary.wiley.com/doi/abs/10.1002/ett.4233

[17] X. You, C. Wang, and J. E. A. Huang, "Towards 6G wireless communication networks: Vision, enabling technologies, and new paradigm shifts," *Sci. China Inf. Sci.*, vol. 64, Nov. 2020, Art. no. 110301.

[18] T. Huang, W. Yang, J. Wu, J. Ma, X. Zhang, and D. Zhang, "A survey on green 6G network: Architecture and technologies," *IEEE Access*, vol. 7, pp. 175758–175768, 2019.

[19] J. Federici and L. Moeller, "Review of terahertz and subterahertz wireless communications," *J. Appl. Phys.*, vol. 107, no. 11, 2010, Art. no. 111101.

[20] T. Kleine-Ostmann and T. Nagatsuma, "A review on terahertz communications research," *J. Infr. Millim. THz Waves*, vol. 32, no. 2, pp. 143–171, Jan. 2011.

[21] I. F. Akyildiz, J. M. Jornet, and C. Han, "Terahertz band: Next frontier for wireless communications," *Phys. Commun.*, vol. 12, no. 7, pp. 16–32, Jan. 2014. [Online]. Available: https://www.sciencedirect.com/science/article/pii/S1874490714000238

[22] H. Sarieddeen, M.-S. Alouini, and T. Y. Al-Naffouri, "An overview of signal processing techniques for terahertz communications," *Proc. IEEE*, vol. 109, no. 10, pp. 1628–1665, Oct. 2021.

[23] D. Headland, Y. Monnai, D. Abbott, C. Fumeaux, and W. Withayachumnankul, "Tutorial: Terahertz beamforming, from concepts to realizations," *APL Photon.*, vol. 3, no. 5, May 2018, Art. no. 051101, doi: 10.1063/1.5011063.

[24] D. M. Mittleman, "Twenty years of terahertz imaging [invited]," *Opt. Exp.*, vol. 26, no. 8, pp. 9417–9431, Apr. 2018. [Online]. Available: http://opg.optica.org/oe/abstract.cfm?URI=oe-26-8-9417

[25] H. Chen, H. Sarieddeen, T. Ballal, H. Wymeersch, M.-S. Alouini, and T. Y. Al-Naffouri, "A tutorial on terahertz-band localization for 6G communication systems," *IEEE Commun. Surveys Tuts.*, vol. 24, no. 3, pp. 1780–1815, 3rd Quart., 2022.

[26] T. Kürner and S. Priebe, "Towards THz communications—Status in research, standardization and regulation," *J. Infr., Millim., THz Waves*, vol. 35, no. 1, pp. 53–62, Jan. 2014.

[27] C. Han, Y. Wang, Y. Li, Y. Chen, N. A. Abbasi, T. Kurner, and A. F. Molisch, "Terahertz wireless channels: A holistic survey on measurement, modeling, and analysis," *IEEE Commun. Surveys Tuts.*, vol. 24, no. 3, pp. 1670–1707, 3rd Quart., 2022.

[28] Y. Lyu, P. Kyösti, and W. Fan, "Sub-terahertz channel sounder: Review and future challenges," *China Commun.*, 2022.

[29] T. S. Rappaport, Y. Xing, O. Kanhere, S. Ju, A. Madanayake, S. Mandal, A. Alkhateeb, and G. C. Trichopoulos, "Wireless communications and applications above 100 GHz: Opportunities and challenges for 6G and beyond," *IEEE Access*, vol. 7, pp. 78729–78757, 2019.

[30] S. Salous, *Radio Propagation Measurement and Channel Modelling*. Hoboken, NJ, USA: Wiley, 2013.

[31] A. Al-Saman, M. Cheffena, O. Elijah, Y. A. Al-Gumaei, S. K. A. Rahim, and T. Al-Hadhrami, "Survey of millimeter-wave propagation measurements and models in indoor environments," *Electronics*, vol. 10, no. 14, p. 1653, Jul. 2021. [Online]. Available: https://www.mdpi.com/2079-9292/10/14/1653

[32] J. Hejselbæk, J. O. Nielsen, C. Drewes, W. Fan, and G. F. Pedersen, "Propagation measurements for device-to-device communication in forest terrain," in *Proc. 12th Eur. Conf. Antennas Propag. (EuCAP)*, 2018, pp. 1–5.

[33] H. Zhao, L. Wei, M. Jarrahi, and G. Pottie, "Propagation measurements for indoor wireless communications at 350/650 GHz," in *Proc. 43rd Int. Conf. Infr., Millim., THz Waves (IRMMW-THz)*, Sep. 2018, pp. 1–2.

[34] R. Takahashi, K. Shibata, and M. Kim, "Development and verification of double-directional channel sounder at 300 GHz," in *Proc. Int. Symp. Antennas Propag. (ISAP)*, Oct. 2022, pp. 523–524.

[35] S. Chakraborty, C. Parisi, D. Saha, and N. Thawdar, "A case for OFDM in ultra-broadband terahertz communication: An experimental approach," in *Proc. 5th ACM Workshop Millim.-Wave THz Netw. Sens. Syst.* New York, NY, USA: Association for Computing Machinery, Oct. 2021, pp. 1–6, doi: 10.1145/3477081.3481671.

[36] P. Sen, V. Ariyarathna, A. Madanayake, and J. M. Jornet, "A versatile experimental testbed for ultrabroadband communication networks above 100 GHz," *Comput. Netw.*, vol. 193, Jul. 2021, Art. no. 108092. [Online]. Available: https://www.sciencedirect.com/science/article/pii/S1389128621001778

[37] P. B. Papazian, K. A. Remley, C. Gentile, and N. Golmie, "A radio channel sounder for mobile millimeter-wave communications: System implementation and measurement assessment," *IEEE Trans. Microw. Theory Techn.*, vol. 64, no. 9, pp. 2924–2932, Sep. 2016.

[38] A. W. Mbugua, W. Fan, Y. Ji, and G. F. Pedersen, "Millimeter wave multi-user performance evaluation based on measured channels with virtual antenna array channel sounder," *IEEE Access*, vol. 6, pp. 12318–12326, 2018.

[39] M. Kim, H. Pham, Y. Chang, and J. Takada, "Development of low-cost 60-GHz millimeter-wave channel sounding system," in *Proc. Global Symp. Millim. Waves (GSMM)*, Apr. 2013, pp. 1–4.

[40] T. Zwick, T. J. Beukema, and H. Nam, "Wideband channel sounder with measurements and model for the 60 GHz indoor radio channel," *IEEE Trans. Veh. Technol.*, vol. 54, no. 4, pp. 1266–1277, Jul. 2005.

[41] R. J. Weiler, M. Peter, T. Kühne, M. Wisotzki, and W. Keusgen, "Simultaneous millimeter-wave multi-band channel sounding in an urban access scenario," in *Proc. 9th Eur. Conf. Antennas Propag. (EuCAP)*, 2015, pp. 1–5.

[42] A. Molisch, *Wireless Communications*. Hoboken, NJ, USA: Wiley, 2011.

[43] R. Zhang, S. Wang, X. Lu, W. Duan, and L. Cai, "Two-dimensional DoA estimation for multipath propagation characterization using the array response of PN-sequences," *IEEE Trans. Wireless Commun.*, vol. 15, no. 1, pp. 341–356, Jan. 2016.

[44] E. L. Cid, M. G. Sanchez, and A. V. Alejos, "High speed transmission at 60 GHz for 5G communications," in *Proc. IEEE Int. Symp. Antennas Propag. USNC/URSI Nat. Radio Sci. Meeting*, Jul. 2015, pp. 1007–1008.

[45] R. J. Pirkl and G. D. Durgin, "Optimal sliding correlator channel sounder design," *IEEE Trans. Wireless Commun.*, vol. 7, no. 9, pp. 3488–3497, Sep. 2008.

[46] H. Cox, "Spatial correlation in arbitrary noise fields with application to ambient sea noise," *J. Acoust. Soc. Amer.*, vol. 54, no. 5, pp. 1289–1301, 1973, doi: 10.1121/1.1914426.

[47] H. Harde, R. A. Cheville, and D. Grischkowsky, "Terahertz studies of collision-broadened rotational lines," *J. Phys. Chem. A*, vol. 101, no. 20, pp. 3646–3660, May 1997.

[48] J. Neu and C. A. Schmuttenmaer, "Tutorial: An introduction to terahertz time domain spectroscopy (THz-TDS)," *J. Appl. Phys.*, vol. 124, no. 23, Dec. 2018, Art. no. 231101, doi: 10.1063/1.5047659.

[49] M. Jacob, S. Priebe, R. Dickhoff, T. Kleine-Ostmann, T. Schrader, and T. Kurner, "Diffraction in mm and sub-mm wave indoor propagation channels," *IEEE Trans. Microw. Theory Techn.*, vol. 60, no. 3, pp. 833–844, Mar. 2012.

[50] R. Piesiewicz, C. Jansen, D. Mittleman, T. Kleine-Ostmann, M. Koch, and T. Kürner, "Scattering analysis for the modeling of THz communication systems," *IEEE Trans. Antennas Propag.*, vol. 55, no. 11, pp. 3002–3009, Nov. 2007.

[51] C. Jansen, R. Piesiewicz, D. Mittleman, T. Kurner, and M. Koch, "The impact of reflections from stratified building materials on the wave propagation in future indoor terahertz communication systems," *IEEE Trans. Antennas Propag.*, vol. 56, no. 5, pp. 1413–1419, May 2008.

[52] C. Jansen, S. Priebe, C. Moller, M. Jacob, H. Dierke, M. Koch, and T. Kurner, "Diffuse scattering from rough surfaces in THz communication channels," *IEEE Trans. THz Sci. Technol.*, vol. 1, no. 2, pp. 462–472, Nov. 2011.

[53] Rhode and Schwartz. *ZVA Vector Network Analyzer*. Accessed: Sep. 16, 2022. [Online]. Available: https://www.rohde-schwarz.com/jp/products/test-and-measurement/network-analyzers/rs-zva-vector-network-analyzer_63493-9660.html

[54] Virginia Diodes. *Virginia Diodes*. Accessed: Sep. 16, 2022. [Online]. Available: https://www.vadiodes.com/en/

[55] N. A. Abbasi, A. Hariharan, A. M. Nair, A. S. Almaiman, F. B. Rottenberg, A. E. Willner, and A. F. Molisch, "Double directional channel measurements for THz communications in an urban environment," in *Proc. IEEE Int. Conf. Commun. (ICC)*, Jun. 2020, pp. 1–6.

[56] M. Wang, J.-F. Wang, Q.-Y. Wu, and Y.-X. Huang, "Research on indoor channel measurement and simulation at 340 GHz," *Acta Phys. Sinica*, vol. 63, no. 15, 2014, Art. no. 154101. [Online]. Available: https://wulixb.iphy.ac.cn/en/article/doi/10.7498/aps.63.154101

[57] M. Kim, K. Kumakura, S. Tang, and H. Tsukada, "Multipath clusters observed in outdoor open square environments at 60 GHz," in *Proc. IEEE 94th Veh. Technol. Conf. (VTC-Fall)*, Sep. 2021, pp. 1–5.

[58] M. Schmieder, M. Peter, R. Askar, I. Komsic, and W. Keusgen, "Measurement and characterization of 28 GHz high-speed train backhaul channels in rural propagation scenarios," in *Proc. 12th Eur. Conf. Antennas Propag. (EuCAP)*, 2018, pp. 1–5.

[59] P. Sen, V. Ariyarathna, A. Madanayake, and J. M. Jornet, "Experimental wireless testbed for ultrabroadband terahertz networks," in *Proc. 14th Int. Workshop Wireless Netw. Testbeds, Exp. Eval. Characterization*. New York, NY, USA: Association for Computing Machinery, Sep. 2020, pp. 48–55, doi: 10.1145/3411276.3412196.

[60] Y. Lyu, P. Kyösti, and W. Fan, "Sub-THz VNA-based channel sounder structure and channel measurements at 100 and 300 GHz," in *Proc. IEEE 32nd Annu. Int. Symp. Pers., Indoor Mobile Radio Commun. (PIMRC)*, Sep. 2021, pp. 1–5.

[61] Y. Xing and T. S. Rappaport, "Propagation measurement system and approach at 140 GHz-moving to 6G and above 100 GHz," in *Proc. IEEE Global Commun. Conf. (GLOBECOM)*, Dec. 2018, pp. 1–6.

[62] G. R. MacCartney and T. S. Rappaport, "A flexible millimeter-wave channel sounder with absolute timing," *IEEE J. Sel. Areas Commun.*, vol. 35, no. 6, pp. 1402–1418, Jun. 2017.

[63] M. Naftaly, R. G. Clarke, D. A. Humphreys, and N. M. Ridler, "Metrology state-of-the-art and challenges in broadband phase-sensitive terahertz measurements," *Proc. IEEE*, vol. 105, no. 6, pp. 1151–1165, Jun. 2017.

[64] M. Naftaly, N. Shoaib, D. Stokes, and N. M. Ridler, "Intercomparison of terahertz dielectric measurements using vector network analyzer and time-domain spectrometer," *J. Infr. Milli. THz Waves*, vol. 37, no. 7, pp. 691–702, Jul. 2016.

[65] Y. Xing, O. Kanhere, S. Ju, and T. S. Rappaport, "Indoor wireless channel properties at millimeter wave and sub-terahertz frequencies," in *Proc. IEEE Global Commun. Conf. (GLOBECOM)*, Dec. 2019, pp. 1–6.

[66] S. Ju, S. H. A. Shah, M. A. Javed, J. Li, G. Palteru, J. Robin, Y. Xing, O. Kanhere, and T. S. Rappaport, "Scattering mechanisms and modeling for terahertz wireless communications," in *Proc. IEEE Int. Conf. Commun. (ICC)*, May 2019, pp. 1–7.

[67] V. Degli-Esposti, F. Fuschini, E. M. Vitucci, and G. Falciasecca, "Measurement and modelling of scattering from buildings," *IEEE Trans. Antennas Propag.*, vol. 55, no. 1, pp. 143–153, Jan. 2007.

[68] M. I. Skolnik, *Introduction to Radar Systems*. New York, NY, USA: McGraw-Hill, 2002.

[69] V. Petrov, J. M. Eckhardt, D. Moltchanov, Y. Koucheryavy, and T. Kurner, "Measurements of reflection and penetration losses in low terahertz band vehicular communications," in *Proc. 14th Eur. Conf. Antennas Propag. (EuCAP)*, Mar. 2020, pp. 1–5.

[70] S. Rey, J. M. Eckhardt, B. Peng, K. Guan, and T. Kurner, "Channel sounding techniques for applications in THz communications: A first correlation based channel sounder for ultra-wideband dynamic channel measurements at 300 GHz," in *Proc. 9th Int. Congr. Ultra Mod. Telecommun. Control Syst. Workshops (ICUMT)*, Nov. 2017, pp. 449–453.

[71] J. M. Eckhardt, V. Petrov, D. Moltchanov, Y. Koucheryavy, and T. Kürner, "Channel measurements and modeling for low-terahertz band vehicular communications," *IEEE J. Sel. Areas Commun.*, vol. 39, no. 6, pp. 1590–1603, Jun. 2021.

[72] S. Ju, Y. Xing, O. Kanhere, and T. S. Rappaport, "Millimeter wave and sub-terahertz spatial statistical channel model for an indoor office building," *IEEE J. Sel. Areas Commun.*, vol. 39, no. 6, pp. 1561–1575, Jun. 2021.

[73] S. Ju, Y. Xing, O. Kanhere, and T. S. Rappaport, "Sub-terahertz channel measurements and characterization in a factory building," in *Proc. IEEE Int. Conf. Commun. (ICC)*, May 2022, pp. 2882–2887.

[74] J. M. Eckhardt, T. Doeker, S. Rey, and T. Kürner, "Measurements in a real data centre at 300 ghz and recent results," in *2019 13th Eur. Conf. Antennas Propag. (EuCAP)*, 2019, pp. 1–5.

[75] R. Müller, R. Herrmann, D. A. Dupleich, C. Schneider, and R. S. Thomä, "Ultrawideband multichannel sounding for mm-wave," in *Proc. 8th Eur. Conf. Antennas Propag. (EuCAP)*, Apr. 2014, pp. 817–821.

[76] D. Dupleich, R. Müller, S. Skoblikov, M. Landmann, G. D. Galdo, and R. Thomä, "Characterization of the propagation channel in conference room scenario at 190 GHz," in *Proc. 14th Eur. Conf. Antennas Propag. (EuCAP)*, Mar. 2020, pp. 1–5.

[77] K. Guan, B. Ai, D. He, F. Zhu, H. Yi, J. Dou, and Z. Zhong, "Channel sounding and ray tracing for THz channel characterization," in *Proc. 13th U.K.-Eur.-China Workshop Millim.-Waves THz Technol. (UCMMT)*, Aug. 2020, pp. 1–3.

[78] K. Guan, B. Peng, D. He, J. M. Eckhardt, S. Rey, B. Ai, Z. Zhong, and T. Kürner, "Channel characterization for intra-wagon communication at 60 and 300 GHz bands," *IEEE Trans. Veh. Technol.*, vol. 68, no. 6, pp. 5193–5207, Jun. 2019.

[79] J. M. Eckhardt, T. Doeker, and T. Kurner, "Indoor-to-outdoor path loss measurements in an aircraft for terahertz communications," in *Proc. IEEE 91st Veh. Technol. Conf. (VTC-Spring)*, May 2020, pp. 1–5.

[80] Y. Xing and T. S. Rappaport, "Propagation measurements and path loss models for sub-THz in urban microcells," in *Proc. IEEE Int. Conf. Commun. (ICC)*, Jun. 2021, pp. 1–6.

[81] O. Kanhere and T. S. Rappaport, "Outdoor sub-THz position location and tracking using field measurements at 142 GHz," in *Proc. IEEE Int. Conf. Commun. (ICC)*, Jun. 2021, pp. 1–6.

[82] S. Ju and T. S. Rappaport, "140 GHz urban microcell propagation measurements for spatial consistency modeling," in *Proc. IEEE Int. Conf. Commun. (ICC)*, Jun. 2021, pp. 1–6.

[83] S. Ju and T. S. Rappaport, "Sub-terahertz spatial statistical MIMO channel model for urban microcells at 142 GHz," in *Proc. IEEE Global Commun. Conf. (GLOBECOM)*, Dec. 2021, pp. 1–6.

[84] F. Undi, A. Schultze, W. Keusgen, M. Peter, and T. Eichler, "Angle-resolved THz channel measurements at 300 GHz in an outdoor environment," in *Proc. IEEE Int. Conf. Commun. Workshops (ICC Workshops)*, Jun. 2021, pp. 1–7.

[85] M. Schmieder, W. Keusgen, M. Peter, S. Wittig, T. Merkle, S. Wagner, M. Kuri, and T. Eichler, "THz channel sounding: Design and validation of a high performance channel sounder at 300 GHz," in *Proc. IEEE Wireless Commun. Netw. Conf. Workshops (WCNCW)*, Apr. 2020, pp. 1–6.

[86] I. Leibowicz, P. Nicolas, and L. Ratton, "Radar/ESM tracking of constant velocity target: Comparison of batch (MLE) and EKF performance," in *Proc. 3rd Int. Conf. Inf. Fusion*, vol. 1, 2000, pp. TUC2/3–TUC2/8.

[87] Q. Yang, D. G. Taylor, and G. D. Durgin, "Kalman filter based localization and tracking estimation for HIMR RFID systems," in *Proc. IEEE Int. Conf. RFID (RFID)*, Apr. 2018, pp. 1–5.

[88] K. Guan, B. Peng, D. He, J. M. Eckhardt, S. Rey, B. Ai, Z. Zhong, and T. Kürner, "Measurement, simulation, and characterization of train-to-infrastructure inside-station channel at the terahertz band," *IEEE Trans. THz Sci. Technol.*, vol. 9, no. 3, pp. 291–306, May 2019.

[89] K. Guan, B. Peng, D. He, D. Yan, B. Ai, Z. Zhong, and T. Kürner, "Channel sounding and ray tracing for train-to-train communications at the THz band," in *Proc. 13th Eur. Conf. Antennas Propag. (EuCAP)*, 2019, pp. 1–5.

[90] K. Guan, D. He, B. Ai, Y. Chen, C. Han, B. Peng, Z. Zhong, and T. Kürner, "Channel characterization and capacity analysis for THz communication enabled smart rail mobility," *IEEE Trans. Veh. Technol.*, vol. 70, no. 5, pp. 4065–4080, May 2021.

[91] T. Kleine-Ostmann, R. Piesiewicz, N. Krumbholz, D. Mittleman, T. Kurner, and M. Koch, "Characterization of building materials for the modeling of pico-cellular THz communication systems," in *Proc. Joint 30th Int. Conf. Infr. Millim. Waves 13th Int. Conf. THz Electron.*, vol. 2, 2005, pp. 592–593.

[92] Z. Hossain, C. N. Mollica, J. F. Federici, and J. M. Jornet, "Stochastic interference modeling and experimental validation for pulse-based terahertz communication," *IEEE Trans. Wireless Commun.*, vol. 18, no. 8, pp. 4103–4115, Aug. 2019.

[93] J. Ma, F. Vorrius, L. Lamb, L. Moeller, and J. F. Federici, "Comparison of experimental and theoretical determined terahertz attenuation in controlled rain," *J. Infr., Millim., THz Waves*, vol. 36, no. 12, pp. 1195–1202, Dec. 2015.

[94] J. F. Federici, J. Ma, and L. Moeller, "Review of weather impact on outdoor terahertz wireless communication links," *Nano Commun. Netw.*, vol. 10, pp. 13–26, Dec. 2016. [Online]. Available: https://www.sciencedirect.com/science/article/pii/S1878778916300394

[95] P. Beckmann and A. Spizzichino, *The Scattering of Electromagnetic Waves From Rough Surfaces*. Norwood, MA, USA: Artech House, 1987.
[96] S. Priebe, M. Jacob, and T. Kuerner, "AoA, AoD and ToA characteristics of scattered multipath clusters for THz indoor channel modeling," in *Proc. 17th Eur. Wireless Sustain. Wireless Technol.*, 2011, pp. 1–9.
[97] J. Federici, L. Moeller, and K. Su, "Terahertz wireless communications," in *Handbook of Terahertz Technology for Imaging, Sensing and Communications* (Woodhead Publishing Series in Electronic and Optical Materials), D. Saeedkia, Ed. Sawston, U.K.: Woodhead Publishing, 2013, pp. 156–214.
[98] Y. Yang, M. Mandehgar, and D. Grischkowsky, "THz-TDS characterization of the digital communication channels of the atmosphere and the enabled applications," *J. Infr., Millim., THz Waves*, vol. 36, no. 2, pp. 97–129, 2015.
[99] K. Su, L. Moeller, R. B. Barat, and J. F. Federici, "Experimental comparison of performance degradation from terahertz and infrared wireless links in fog," *J. Opt. Soc. Amer. A, Opt. Image Sci.*, vol. 29, no. 2, pp. 179–184, Feb. 2012. [Online]. Available: http://opg.optica.org/josaa/abstract.cfm?URI=josaa-29-2-179
[100] Y. Yang, M. Mandehgar, and D. R. Grischkowsky, "Broadband THz signals propagate through dense fog," *IEEE Photon. Technol. Lett.*, vol. 27, no. 4, pp. 383–386, Feb. 15, 2015.
[101] K. Su, L. Moeller, R. B. Barat, and J. F. Federici, "Experimental comparison of terahertz and infrared data signal attenuation in dust clouds," *J. Opt. Soc. Amer. A, Opt. Image Sci.*, vol. 29, no. 11, pp. 2360–2366, Nov. 2012. [Online]. Available: http://opg.optica.org/josaa/abstract.cfm?URI=josaa-29-11-2360
[102] J. Ma, L. Moeller, and J. F. Federici, "Experimental comparison of terahertz and infrared signaling in controlled atmospheric turbulence," *J. Infr., Millim., THz Waves*, vol. 36, no. 2, pp. 130–143, Feb. 2015.
[103] D. Long and F. T. Ulaby, *Microwave Radar and Radiometric Remote Sensing*. Norwood, MA, USA: Artech House, 2015.
[104] G. A. Siles, J. M. Riera, and P. Garcia-del-Pino, "Atmospheric attenuation in wireless communication systems at millimeter and THz frequencies [wireless corner]," *IEEE Antennas Propag. Mag.*, vol. 57, no. 1, pp. 48–61, Feb. 2015.
[105] B. Wu, B. Marchant, and M. Kavehrad, "Channel modeling of light signals propagating through a battlefield environment: Analysis of channel spatial, angular, and temporal dispersion," *Appl. Opt.*, vol. 46, pp. 6442–6448, Sep. 2007. [Online]. Available: http://opg.optica.org/ao/abstract.cfm?URI=ao-46-25-6442
[106] A. C. Best, "The size distribution of raindrops," *Quart. J. Roy. Meteorol. Soc.*, vol. 76, no. 327, pp. 16–36, Jan. 1950. [Online]. Available: https://rmets.onlinelibrary.wiley.com/doi/abs/10.1002/qj.49707632704
[107] O. Wilfert and L. Dordová, "Calculation and comparison of turbulence attenuation by different methods," *Radioengineering*, vol. 19, no. 1, pp. 162–167, 2010.
[108] S. L. H. Nguyen, J. Järveläinen, A. Karttunen, K. Haneda, and J. Putkonen, "Comparing radio propagation channels between 28 and 140 GHz bands in a shopping mall," in *Proc. 12th Eur. Conf. Antennas Propag. (EuCAP)*, 2018, pp. 1–5.
[109] M. Lotti, M. Caillet, and R. D'Errico, "Comparison of indoor channel characteristics for sub-THz bands from 125 GHz to 300 GHz," in *Proc. 16th Eur. Conf. Antennas Propag. (EuCAP)*, Mar. 2022, pp. 1–5.
[110] L. Pometcu and R. D'Errico, "An indoor channel model for high data-rate communications in D-band," *IEEE Access*, vol. 8, pp. 9420–9433, 2020.
[111] S. L. H. Nguyen, K. Haneda, J. Järveläinen, A. Karttunen, and J. Putkonen, "Large-scale parameters of spatio-temporal short-range indoor backhaul channels at 140 GHz," in *Proc. IEEE 93rd Veh. Technol. Conf. (VTC-Spring)*, Apr. 2021, pp. 1–6.
[112] S. Kim, W. T. Khan, A. Zajić, and J. Papapolymerou, "D-band channel measurements and characterization for indoor applications," *IEEE Trans. Antennas Propag.*, vol. 63, no. 7, pp. 3198–3207, Jul. 2015.
[113] C.-L. Cheng, S. Kim, and A. Zajic, "Comparison of path loss models for indoor 30 GHz, 140 GHz, and 300 GHz channels," in *Proc. 11th Eur. Conf. Antennas Propag. (EUCAP)*, Mar. 2017, pp. 716–720.
[114] S. Kim and A. G. Zajić, "Statistical characterization of 300-GHz propagation on a desktop," *IEEE Trans. Veh. Technol.*, vol. 64, no. 8, pp. 3330–3338, Aug. 2015.
[115] J. He, Y. Chen, Y. Wang, Z. Yu, and C. Han, "Channel measurement and path-loss characterization for low-terahertz indoor scenarios," in *Proc. IEEE Int. Conf. Commun. Workshops (ICC Workshops)*, Jun. 2021, pp. 1–6.
[116] N. Khalid, N. A. Abbasi, and O. B. Akan, "Statistical characterization and analysis of low-THz communication channel for 5G Internet of Things," *Nano Commun. Netw.*, vol. 22, Dec. 2019, Art. no. 100258. [Online]. Available: https://www.sciencedirect.com/science/article/pii/S1878778918300802
[117] S. Priebe, C. Jastrow, M. Jacob, T. Kleine-Ostmann, T. Schrader, and T. Kurner, "Channel and propagation measurements at 300 GHz," *IEEE Trans. Antennas Propag.*, vol. 59, no. 5, pp. 1688–1698, May 2011.
[118] Y. Zantah, M. Alissa, T. Kreul, and T. Kaiser, "Ultra-wideband multipath channel characterization at 300 GHz," in *Proc. 24th Int. ITG Workshop Smart Antennas (WSA)*, 2020, pp. 1–5.
[119] Z. Yu, Y. Chen, G. Wang, W. Gao, and C. Han, "Wideband channel measurements and temporal-spatial analysis for terahertz indoor communications," in *Proc. IEEE Int. Conf. Commun. Workshops (ICC Workshops)*, Jun. 2020, pp. 1–6.
[120] Y. Chen, C. Han, Z. Yu, and G. Wang, "140 GHz channel measurement and characterization in an office room," in *Proc. IEEE Int. Conf. Commun. (ICC)*, Jun. 2021, pp. 1–6.
[121] Y. Chen, Y. Li, C. Han, Z. Yu, and G. Wang, "Channel measurement and ray-tracing-statistical hybrid modeling for low-terahertz indoor communications," *IEEE Trans. Wireless Commun.*, vol. 20, no. 12, pp. 8163–8176, Dec. 2021.
[122] N. A. Abbasi, A. Hariharan, A. M. Nair, and A. F. Molisch, "Channel measurements and path loss modeling for indoor THz communication," in *Proc. 14th Eur. Conf. Antennas Propag. (EuCAP)*, Mar. 2020, pp. 1–5.
[123] N. Khalid and O. B. Akan, "Wideband THz communication channel measurements for 5G indoor wireless networks," in *Proc. IEEE Int. Conf. Commun. (ICC)*, May 2016, pp. 1–6.
[124] D. Serghiou, M. Khalily, S. Johny, M. Stanley, I. Fatadin, T. W. C. Brown, N. Ridler, and R. Tafazolli, "Ultra-wideband terahertz channel propagation measurements from 500 to 750 GHz," in *Proc. Int. Conf. U.K.-China Emerg. Technol. (UCET)*, Aug. 2020, pp. 1–4.
[125] N. Khalid and O. B. Akan, "Experimental throughput analysis of low-THz MIMO communication channel in 5G wireless networks," *IEEE Wireless Commun. Lett.*, vol. 5, no. 6, pp. 616–619, Dec. 2016.
[126] S. Priebe, M. Kannicht, M. Jacob, and T. Kürner, "Ultra broadband indoor channel measurements and calibrated ray tracing propagation modeling at THz frequencies," *J. Commun. Netw.*, vol. 15, no. 6, pp. 547–558, 2013.
[127] Y. Zantah, F. Sheikh, A. A. Abbas, M. Alissa, and T. Kaiser, "Channel measurements in lecture room environment at 300 GHz," in *Proc. 2nd Int. Workshop Mobile THz Syst. (IWMTS)*, Jul. 2019, pp. 1–5.
[128] C.-L. Cheng, S. Sangodoyin, and A. Zajic, "THz cluster-based modeling and propagation characterization in a data center environment," *IEEE Access*, vol. 8, pp. 56544–56558, 2020.
[129] C.-L. Cheng, S. Sangodoyin, and A. Zajic, "Terahertz MIMO fading analysis and Doppler modeling in a data center environment," in *Proc. 14th Eur. Conf. Antennas Propag. (EuCAP)*, Mar. 2020, pp. 1–5.
[130] C.-L. Cheng and A. Zajic, "Characterization of propagation phenomena relevant for 300 GHz wireless data center links," *IEEE Trans. Antennas Propag.*, vol. 68, no. 2, pp. 1074–1087, Feb. 2020.
[131] S. Kim and A. Zajić, "Characterization of 300-GHz wireless channel on a computer motherboard," *IEEE Trans. Antennas Propag.*, vol. 64, no. 12, pp. 5411–5423, Dec. 2016.
[132] H.-J. Song, "LOS channel response measurement at 300 GHz for short-range wireless communication," in *Proc. IEEE Wireless Commun. Netw. Conf. Workshops (WCNCW)*, Apr. 2020, pp. 1–3.
[133] N. A. Abbasi, J. Gomez-Ponce, S. M. Shaikbepari, S. Rao, R. Kondaveti, S. Abu-Surra, G. Xu, C. Zhang, and A. F. Molisch, "Ultra-wideband double directional channel measurements for THz communications in urban environments," in *Proc. IEEE Int. Conf. Commun. (ICC)*, Jun. 2021, pp. 1–6.
[134] N. A. Abbasi, J. Gomez-Ponce, R. Kondaveti, S. M. Shaikbepari, S. Rao, S. Abu-Surra, G. Xu, C. Zhang, and A. F. Molisch, "THz band channel measurements and statistical modeling for urban D2D environments," *IEEE Trans. Wireless Commun.*, early access, Jun. 28, 2022, doi: 10.1109/TWC.2022.3184929.
[135] N. A. Abbasi, J. Gomez-Ponce, D. Burghal, R. Kondaveti, S. Abu-Surra, G. Xu, C. Zhang, and A. F. Molisch, "Double-directional channel measurements for urban THz communications on a linear route," in *Proc. IEEE Int. Conf. Commun. Workshops (ICC Workshops)*, Jun. 2021, pp. 1–6.

[136] R. Piesiewicz, T. Kleine-Ostmann, N. Krumbholz, D. Mittleman, M. Koch, J. Schoebel, and T. Kurner, "Short-range ultra-broadband terahertz communications: Concepts and perspectives," *IEEE Antennas Propag. Mag.*, vol. 49, no. 6, pp. 24–39, Dec. 2007.

[137] M. Koch, "Terahertz communications: A 2020 vision," in *Terahertz Frequency Detection and Identification of Materials and Objects*, R. E. Miles, X.-C. Zhang, H. Eisele, and A. Krotkus, Eds. Dordrecht, The Netherlands: Springer, 2007, pp. 325–338.

[138] K. Guan, G. Li, T. Kürner, A. F. Molisch, B. Peng, R. He, B. Hui, J. Kim, and Z. Zhong, "On millimeter wave and THz mobile radio channel for smart rail mobility," *IEEE Trans. Veh. Technol.*, vol. 66, no. 7, pp. 5658–5674, Jul. 2017.

[139] M. Kim, S. Tang, and K. Kumakura, "Fast double-directional full azimuth sweep channel sounder using low-cost COTS beamforming RF transceivers," *IEEE Access*, vol. 9, pp. 80288–80299, 2021.

[140] K. Kumakura, S. Tang, H. Tsukada, and M. Kim, "Large scale characteristics of millimeter-wave propagation channels in various indoor office environments," in *Proc. Int. Symp. Antennas Propag. (ISAP)*, Oct. 2021, pp. 1–2.

[141] H. Tsukada, K. Kumakura, S. Tang, and M. Kim, "Millimeter-wave channel model parameters for various office environments," *IEEE Access*, vol. 10, pp. 60387–60396, 2022.

[142] M. Kim, S. Kishimoto, S. Yamakawa, and K. Guan, "Millimeter-wave intra-cluster channel model for in-room access scenarios," *IEEE Access*, vol. 8, pp. 82042–82053, 2020.

[143] C. Han and Y. Chen, "Propagation modeling for wireless communications in the terahertz band," *IEEE Commun. Mag.*, vol. 56, no. 6, pp. 96–101, Jun. 2018.

[144] I. F. Akyildiz and J. M. Jornet, "Realizing ultra-massive MIMO (1024 × 1024) communication in the (0.06–10) terahertz band," *Nano Commun. Netw.*, vol. 8, pp. 46–54, Jun. 2016. [Online]. Available: https://www.sciencedirect.com/science/article/pii/S1878778916000107

[145] C. Han, A. O. Bicen, and I. F. Akyildiz, "Multi-ray channel modeling and wideband characterization for wireless communications in the terahertz band," *IEEE Trans. Wireless Commun.*, vol. 14, no. 5, pp. 2402–2412, May 2015.

[146] S. Priebe and T. Kürner, "Stochastic modeling of THz indoor radio channels," *IEEE Trans. Wireless Commun.*, vol. 12, no. 9, pp. 4445–4455, Sep. 2013.

[147] A. F. Molisch, "A generic model for MIMO wireless propagation channels in macro- and microcells," *IEEE Trans. Signal Process.*, vol. 52, no. 1, pp. 61–71, Jan. 2004.

[148] L. Bai, C.-X. Wang, J. Huang, Q. Xu, Y. Yang, G. Goussetis, J. Sun, and W. Zhang, "Predicting wireless mmWave massive MIMO channel characteristics using machine learning algorithms," *Wireless Commun. Mobile Comput.*, vol. 2018, pp. 1–12, Aug. 2018.

[149] P.-R. Chang and W.-H. Yang, "Environment-adaptation mobile radio propagation prediction using radial basis function neural networks," in *Proc. 4th IEEE Int. Conf. Universal Pers. Commun. (ICUPC)*, Nov. 1995, pp. 278–282.

[150] J. Huang, C.-X. Wang, L. Bai, J. Sun, Y. Yang, J. Li, O. Tirkkonen, and M.-T. Zhou, "A big data enabled channel model for 5G wireless communication systems," *IEEE Trans. Big Data*, vol. 6, no. 2, pp. 211–222, Jun. 2020.

[151] X. Zhao, F. Du, S. Geng, Z. Fu, Z. Wang, Y. Zhang, Z. Zhou, L. Zhang, and L. Yang, "Playback of 5G and beyond measured MIMO channels by an ANN-based modeling and simulation framework," *IEEE J. Sel. Areas Commun.*, vol. 38, no. 9, pp. 1945–1954, Sep. 2020.

[152] Q. Zhang, A. Ferdowsi, and W. Saad, "Distributed generative adversarial networks for mmWave channel modeling in wireless UAV networks," in *Proc. IEEE Int. Conf. Commun. (ICC)*, Jun. 2021, pp. 1–6.

[153] T. J. O'Shea, T. Roy, and N. West, "Approximating the void: Learning stochastic channel models from observation with variational generative adversarial networks," in *Proc. Int. Conf. Comput., Netw. Commun. (ICNC)*, Feb. 2019, pp. 681–686.

[154] K. Mao, Q. Zhu, M. Song, H. Li, B. Ning, G. F. Pedersen, and W. Fan, "Machine-learning-based 3-D channel modeling for U2V mmWave communications," *IEEE Internet Things J.*, vol. 9, no. 18, pp. 17592–17607, Sep. 2022.

[155] W. Xia, S. Rangan, M. Mezzavilla, A. Lozano, G. Geraci, V. Semkin, and G. Loianno, "Generative neural network channel modeling for millimeter-wave UAV communication," *IEEE Trans. Wireless Commun.*, vol. 21, no. 11, pp. 9417–9431, Nov. 2022.

[156] W. Xia, S. Rangan, M. Mezzavilla, A. Lozano, G. Geraci, V. Semkin, and G. Loianno, "Millimeter wave channel modeling via generative neural networks," in *Proc. IEEE Globecom Workshops (GC Wkshps*, Dec. 2020, pp. 1–6.

[157] T. K. Sarkar, Z. Ji, K. Kim, A. Medouri, and M. Salazar-Palma, "A survey of various propagation models for mobile communication," *IEEE Antennas Propag. Mag.*, vol. 45, no. 3, pp. 51–82, Jun. 2003.

[158] A. Goldsmith, *Wireless Communications*. Cambridge, U.K.: Cambridge Univ. Press, 2005.

[159] S. Y. Seidel and T. S. Rappaport, "Site-specific propagation prediction for wireless in-building personal communication system design," *IEEE Trans. Veh. Technol.*, vol. 43, no. 4, pp. 879–891, Nov. 1994.

[160] W. Honcharenko, H. Bertoni, J. Dailing, J. Qian, and H. Yee, "Mechanisms governing uhf propagation on single floors in modern office buildings," *IEEE Trans. Veh. Technol.*, vol. 41, no. 4, pp. 496–504, Nov. 1992.

[161] W. Seesai, M. Chamchoy, and S. Promwong, "A body-shadowing model for indoor UWB communication environments," in *Proc. 5th Int. Conf. Electr. Eng./Electron., Comput., Telecommun. Inf. Technol.*, vol. 1, May 2008, pp. 261–264.

[162] H.-W. Son and N.-H. Myung, "A deterministic ray tube method for microcellular wave propagation prediction model," *IEEE Trans. Antennas Propag.*, vol. 47, no. 8, pp. 1344–1350, Aug. 1999.

[163] G. Kondylis, F. De Flaviis, G. Pottie, and Y. Rahmat-Samii, "Indoor channel characterization for wireless communications using reduced finite difference time domain (R-FDTD)," in *Proc. Gateway 21st Century Commun. Village (VTC-Fall) IEEE VTS 50th Veh. Technol. Conf.*, vol. 3, Sep. 1999, pp. 1402–1406.

[164] A. Lauer, I. Wolff, A. Bahr, J. Pamp, J. Kunisch, and I. Wolff, "Multimode FDTD simulations of indoor propagation including antenna properties," in *Proc. IEEE 45th Veh. Technol. Conf. Countdown Wireless 21st Century*, vol. 1, Jul. 1995, pp. 454–458.

[165] Y. Wang, S. Safavi-Naeini, and S. K. Chaudhuri, "A hybrid technique based on combining ray tracing and FDTD methods for site-specific modeling of indoor radio wave propagation," *IEEE Trans. Antennas Propag.*, vol. 48, no. 5, pp. 743–754, May 2000.

[166] K. Yee, "Numerical solution of initial boundary value problems involving Maxwell's equations in isotropic media," *IEEE Trans. Antennas Propag.*, vol. AP-14, no. 3, pp. 302–307, May 1966.

[167] A. Taflove and S. C. Hagness, *Computational Electrodynamics: The Finite-Difference Time-Domain Method*. Norwood, MA, USA: Artech House, 2005.

[168] Y. Zhao, Y. Hao, and C. Parini, "FDTD characterisation of UWB indoor radio channel including frequency dependent antenna directivities," in *Proc. Eur. Conf. Wireless Technol.*, Sep. 2006, pp. 298–301.

[169] C.-F. Yang and C.-J. Ko, "A ray tracing method for modeling indoor wave propagation and penetration," in *IEEE Antennas Propag. Soc. Int. Symp. Dig.*, vol. 1, Jul. 1996, pp. 441–444.

[170] B. De Backer, H. Borjeson, F. Olyslager, and D. De Zutter, "The study of wave-propagation through a windowed wall at 1.8 GHz," in *Proc. Veh. Technol. Conf.*, vol. 1, 1996, pp. 165–169.

[171] H. Ragheb and E. R. Hancock, "The modified Beckmann–Kirchhoff scattering theory for rough surface analysis," *Pattern Recognit.*, vol. 40, no. 7, pp. 2004–2020, Jul. 2007. [Online]. Available: https://www.sciencedirect.com/science/article/pii/S0031320306004171

[172] P. Kreuzgruber, P. Unterberger, and R. Gahleitner, "A ray splitting model for indoor radio propagation associated with complex geometries," in *Proc. IEEE 43rd Veh. Technol. Conf.*, May 1993, pp. 227–230.

[173] Z. Jacob, "Quantum plasmonics," *MRS Bull.*, vol. 37, no. 8, pp. 761–767, 2012.

[174] R. R. Saadane and M. Wahbi, "UWB indoor radio propagation modelling in presence of human body shadowing using ray tracing technique," *Int. J. Commun. Netw. Inf. Secur.*, vol. 4, no. 2, p. 132, Apr. 2022.

[175] G. Durgin, N. Patwari, and T. Rappaport, "An advanced 3D ray launching method for wireless propagation prediction," in *Proc. IEEE 47th Veh. Technol. Conf. Technol. Motion*, vol. 2, May 1997, pp. 785–789.

[176] D. M. Rose and T. Kurner, "An analytical 3D ray-launching method using arbitrary polygonal shapes for wireless propagation prediction," in *Proc. IEEE 80th Veh. Technol. Conf. (VTC-Fall)*, Sep. 2014, pp. 1–6.

[177] J. W. McKown and R. L. Hamilton, "Ray tracing as a design tool for radio networks," *IEEE Netw.*, vol. 5, no. 6, pp. 27–30, Nov. 1991.

[178] K. Rizk, J.-F. Wagen, and F. Gardiol, "Two-dimensional ray-tracing modeling for propagation prediction in microcellular environments," *IEEE Trans. Veh. Technol.*, vol. 46, no. 2, pp. 508–518, May 1997.

[179] S.-H. Chen and S.-K. Jeng, "SBR image approach for radio wave propagation in tunnels with and without traffic," *IEEE Trans. Veh. Technol.*, vol. 45, no. 3, pp. 570–578, Aug. 1996.

[180] S.-H. Chen and S.-K. Jeng, "An SBR/image approach for radio wave propagation in indoor environments with metallic furniture," *IEEE Trans. Antennas Propag.*, vol. 45, no. 1, pp. 98–106, Jan. 1997.

[181] K. Ng, E. Tameh, and A. Nix, "Modelling and performance prediction for multiple antenna systems using enhanced ray tracing," in *Proc. IEEE Wireless Commun. Netw. Conf.*, vol. 2, Mar. 2005, pp. 933–937.

[182] A. F. Molisch, "Modeling of directional wireless propagation channels," *URSI Radio Sci. Bull.*, vol. 2002, no. 302, pp. 16–26, Sep. 2002.

[183] J. Järveläinen, K. Haneda, and A. Karttunen, "Indoor propagation channel simulations at 60 GHz using point cloud data," *IEEE Trans. Antennas Propag.*, vol. 64, no. 10, pp. 4457–4467, Oct. 2016.

[184] J. Järveläinen, S. L. H. Nguyen, K. Haneda, R. Naderpour, and U. T. Virk, "Evaluation of millimeter-wave line-of-sight probability with point cloud data," *IEEE Wireless Commum. Lett.*, vol. 5, no. 3, pp. 228–231, Jun. 2016.

[185] U. T. Virk, S. L. H. Nguyen, K. Haneda, and J.-F. Wagen, "On-site permittivity estimation at 60 GHz through reflecting surface identification in the point cloud," *IEEE Trans. Antennas Propag.*, vol. 66, no. 7, pp. 3599–3609, Jul. 2018.

[186] J. Pascual-García, J. M. Molina-García-Pardo, M. T. Martínez-Inglés, J. V. Rodríguez, and N. Saurín-Serrano, "On the importance of diffuse scattering model parameterization in indoor wireless channels at mm-wave frequencies," *IEEE Access*, vol. 4, pp. 688–701, 2016.

[187] J. Pascual-Garcia, J.-M. Molina-Garcia-Pardo, M.-T. Martinez-Ingles, J.-V. Rodriguez, and L. Juan-Llacer, "Wireless channel simulation using geometrical models extrated from point clouds," in *Proc. IEEE Int. Symp. Antennas Propag. USNC/URSI Nat. Radio Sci. Meeting*, Jul. 2018, pp. 83–84.

[188] E. N. Papasotiriou, A.-A.-A. Boulogeorgos, K. Haneda, M. F. de Guzman, and A. Alexiou, "An experimentally validated fading model for THz wireless systems," *Sci. Rep.*, vol. 11, no. 1, Sep. 2021, Art. no. 18717.

[189] G. Gougeon, Y. Corre, and M. Z. Aslam, "Ray-based deterministic channel modelling for sub-THz band," in *Proc. IEEE 30th Int. Symp. Pers., Indoor Mobile Radio Commun. (PIMRC Workshops)*, Sep. 2019, pp. 1–6.

[190] F. Sheikh, D. Lessy, and T. Kaiser, "A novel ray-tracing algorithm for non-specular diffuse scattered rays at terahertz frequencies," in *Proc. 1st Int. Workshop Mobile THz Syst. (IWMTS)*, Jul. 2018, pp. 1–6.

[191] F. Sheikh, Y. Gao, and T. Kaiser, "A study of diffuse scattering in massive MIMO channels at terahertz frequencies," *IEEE Trans. Antennas Propag.*, vol. 68, no. 2, pp. 997–1008, Feb. 2020.

[192] C. Han and I. F. Akyildiz, "Three-dimensional end-to-end modeling and analysis for graphene-enabled terahertz band communications," *IEEE Trans. Veh. Technol.*, vol. 66, no. 7, pp. 5626–5634, Jul. 2017.

[193] C.-X. Yuan, Z.-X. Zhou, J. W. Zhang, X.-L. Xiang, F. Yue, and H.-G. Sun, "FDTD analysis of terahertz wave propagation in a high-temperature unmagnetized plasma slab," *IEEE Trans. Plasma Sci.*, vol. 39, no. 7, pp. 1577–1584, Jul. 2011.

[194] M. Y. Wang, M. Zhang, G. P. Li, B. J. Jiang, X. C. Zhang, and J. Xu, "FDTD simulation on terahertz waves propagation through a dusty plasma," *Plasma Sci. Technol.*, vol. 18, no. 8, pp. 798–803, Aug. 2016, doi: 10.1088/1009-0630/18/8/02.

[195] W. Yan, D. Chen, F. Kong, and X. Bai, "FDTD simulation of terahertz wave propagation in time-varying plasma," in *Proc. Photon. Electromagn. Res. Symp. Fall (PIERS Fall)*, Dec. 2019, pp. 699–701.

[196] W.-L. Tu, S.-C. Zhong, H.-Z. Yao, and Y.-C. Shen, "FDTD-based computed terahertz wave propagation in multilayer medium structures," *Proc. SPIE*, vol. 8909, pp. 217–225, Aug. 2013, doi: 10.1117/12.2034515.

[197] A. Fricke, C. Homann, and T. Kurner, "Time-domain propagation investigations for terahertz intra-device communications," in *Proc. 8th Eur. Conf. Antennas Propag. (EuCAP)*, Apr. 2014, pp. 1760–1764.

[198] Z. Sandor, L. Nagy, Z. Szabo, and T. Csaba, "3D ray launching and moment method for indoor radio propagation purposes," in *Proc. 8th Int. Symp. Pers., Indoor Mobile Radio Commun. (PIMRC)*, vol. 1, 1997, pp. 130–134.

[199] C.-F. Yang and B.-C. Wu, "Simulations and measurements for indoor wave propagation through periodic structures," in *IEEE Antennas Propag. Soc. Int. Symp. Dig. Held Conjunct USNC/URSI Nat. Radio Sci. Meeting*, vol. 1, Jul. 1999, pp. 384–387.

[200] C.-F. Yang and T.-S. Wang, "A moment method solution for determining the shielding and scattering properties of two-dimensional objects above a lossy half space," in *Proc. Int. Symp. Electromagn. Compat.*, 1995, pp. 630–635.

[201] P. Almers, E. Bonek, A. Burr, N. Czink, M. Debbah, V. Degli-Esposti, H. Hofstetter, P. Kyösti, D. Laurenson, G. Matz, A. F. Molisch, C. Oestges, and H. Özcelik, "Survey of channel and radio propagation models for wireless MIMO systems," *EURASIP J. Wireless Commun. Netw.*, vol. 2007, no. 1, Dec. 2007, Art. no. 019070.

[202] A. F. Molisch, A. Kuchar, J. Laurila, K. Hugl, and R. Schmalenberger, "Geometry-based directional model for mobile radio channels—Principles and implementation," *Eur. Trans. Telecommun.*, vol. 14, no. 4, pp. 351–359, 2003. [Online]. Available: https://onlinelibrary.wiley.com/doi/abs/10.1002/ett.928

[203] J. J. Blanz and P. Jung, "A flexibly configurable spatial model for mobile radio channels," *IEEE Trans. Commun.*, vol. 46, no. 3, pp. 367–371, Mar. 1998.

[204] O. Norklit and J. Andersen, "Diffuse channel model and experimental results for array antennas in mobile environments," *IEEE Trans. Antennas Propag.*, vol. 46, no. 6, pp. 834–840, Jun. 1998.

[205] J. Fuhl, A. F. Molisch, and E. Bonek, "Unified channel model for mobile radio systems with smart antennas," *IEE Proc., Radar, Sonar Navigat.*, vol. 145, no. 1, pp. 32–41, Feb. 1998. [Online]. Available: https://digital-library.theiet.org/content/journals/10.1049/ip-rsn_19981750

[206] P. Petrus, J. H. Reed, and T. S. Rappaport, "Geometrical-based statistical macrocell channel model for mobile environments," *IEEE Trans. Commun.*, vol. 50, no. 3, pp. 495–502, Mar. 2002.

[207] Y. Huang, H. Chang, J. Huang, W. Zhang, J. Sun, and C.-X. Wang, "A 3D wideband GBSM for THz communications in indoor scenarios," in *Proc. 11th Int. Conf. Wireless Commun. Signal Process. (WCSP)*, Oct. 2019, pp. 1–6.

[208] J. Wang, C.-X. Wang, J. Huang, H. Wang, X. Gao, X. You, and Y. Hao, "A novel 3D non-stationary GBSM for 6G THz ultra-massive MIMO wireless systems," 2021, *arXiv:2108.06542*.

[209] T. Zwick, C. Fischer, D. Didascalou, and W. Wiesbeck, "A stochastic spatial channel model based on wave-propagation modeling," *IEEE J. Sel. Areas Commun.*, vol. 18, no. 1, pp. 6–15, Jan. 2000.

[210] T. Zwick, C. Fischer, and W. Wiesbeck, "A stochastic multipath channel model including path directions for indoor environments," *IEEE J. Sel. Areas Commun.*, vol. 20, no. 6, pp. 1178–1192, Aug. 2002.

[211] M. Kim, "Analysis of multipath component parameter estimation accuracy in directional scanning measurement," *IEEE Antennas Wireless Propag. Lett.*, vol. 17, no. 1, pp. 12–16, Jan. 2018.

[212] A. F. Molisch, "Ultrawideband propagation channels-theory, measurement, and modeling," *IEEE Trans. Veh. Technol.*, vol. 54, no. 5, pp. 1528–1545, Sep. 2005.

[213] A. L. Imoize, A. E. Ibhaze, A. A. Atayero, and K. V. N. Kavitha, "Standard propagation channel models for MIMO communication systems," *Wireless Commun. Mobile Comput.*, vol. 2021, pp. 1–36, Feb. 2021.

[214] J.-P. Kermoal, L. Schumacher, K. I. Pedersen, P. E. Mogensen, and F. Frederiksen, "A stochastic MIMO radio channel model with experimental validation," *IEEE J. Sel. Areas Commun.*, vol. 20, no. 6, pp. 1211–1226, Aug. 2002.

[215] T. Svantesson and J. W. Wallace, "Tests for assessing multivariate normality and the covariance structure of MIMO data," in *Proc. IEEE Int. Conf. Acoust., Speech, Signal Process. (ICASSP)*, vol. 4, Apr. 2003, p. 656.

[216] C. Oestges, "Validity of the Kronecker model for MIMO correlated channels," in *Proc. IEEE 63rd Veh. Technol. Conf.*, vol. 6, May 2006, pp. 2818–2822.

[217] A. M. Sayeed, "Deconstructing multiantenna fading channels," *IEEE Trans. Signal Process.*, vol. 50, no. 10, pp. 2563–2579, Oct. 2002.

[218] L. You, X. Gao, G. Y. Li, X.-G. Xia, and N. Ma, "BDMA for millimeter-wave/terahertz massive MIMO transmission with per-beam synchronization," *IEEE J. Sel. Areas Commun.*, vol. 35, no. 7, pp. 1550–1563, Jul. 2017.

[219] C. Sun, X. Q. Gao, S. Jin, M. Matthaiou, Z. Ding, and C. Xiao, "Beam division multiple access transmission for massive MIMO communications," *IEEE Trans. Commun.*, vol. 63, no. 6, pp. 2170–2184, Jun. 2015.

[220] W. Weichselberger, M. Herdin, H. Ozcelik, and E. Bonek, "A stochastic MIMO channel model with joint correlation of both link ends," *IEEE Trans. Wireless Commun.*, vol. 5, no. 1, pp. 90–100, Jan. 2006.

[221] W. Saad, M. Bennis, and M. Chen, "A vision of 6G wireless systems: Applications, trends, technologies, and open research problems," *IEEE Netw.*, vol. 34, no. 3, pp. 134–142, May/Jun. 2020.

[222] R. U. Nabar, H. Bolcskei, V. Erceg, D. Gesbert, and A. J. Paulraj, "Performance of multiantenna signaling techniques in the presence of polarization diversity," *IEEE Trans. Signal Process.*, vol. 50, no. 10, pp. 2553–2562, Oct. 2002.

[223] W. Xu, S. A. Zekavat, and H. Tong, "A novel spatially correlated multiuser MIMO channel modeling: Impact of surface roughness," *IEEE Trans. Antennas Propag.*, vol. 57, no. 8, pp. 2429–2438, Aug. 2009.

[224] M. Katzin, "The scattering of electromagnetic waves from rough surfaces," *Proc. IEEE*, vol. 52, no. 11, pp. 1389–1390, Nov. 1964.

[225] J. Gong, J. F. Hayes, and M. R. Soleymani, "The effect of antenna physics on fading correlation and the capacity of multielement antenna systems," in *Proc. Can. Conf. Electr. Comput. Eng.*, 2005, pp. 1363–1366.

[226] A. Abdi and M. Kaveh, "Space-time correlation modeling of multielement antenna systems in mobile fading channels," in *Proc. IEEE Int. Conf. Acoust., Speech, Signal Process.*, vol. 4, May 2001, pp. 2505–2508.

[227] A. Amar, "The effect of local scattering on the gain and beamwidth of a collaborative beampattern for wireless sensor networks," *IEEE Trans. Wireless Commun.*, vol. 9, no. 9, pp. 2730–2736, Sep. 2010.

[228] C. Oestges, B. Clerckx, D. Vanhoenacker-Janvier, and A. J. Paulraj, "Impact of fading correlations on MIMO communication systems in geometry-based statistical channel models," *IEEE Trans. Wireless Commun.*, vol. 4, no. 3, pp. 1112–1120, May 2005.

[229] Y. Choi, J.-W. Choi, and J. M. Cioffi, "A geometric-statistic channel model for THz indoor communications," *J. Infr., Millim., THz Waves*, vol. 34, nos. 7–8, pp. 456–467, Aug. 2013.

[230] A. A. M. Saleh and R. A. Valenzuela, "A statistical model for indoor multipath propagation," *IEEE J. Sel. Areas Commun.*, vol. SAC-5, no. 2, pp. 128–137, Feb. 1987.

[231] G. L. Turin, F. D. Clapp, T. L. Johnston, S. B. Fine, and D. Lavry, "A statistical model of urban multipath propagation," *IEEE Trans. Veh. Technol.*, vol. VT-21, no. 1, pp. 1–9, Feb. 1972.

[232] M. K. Samimi and T. S. Rappaport, "3-D statistical channel model for millimeter-wave outdoor mobile broadband communications," in *Proc. IEEE Int. Conf. Commun. (ICC)*, Jun. 2015, pp. 2430–2436.

[233] P. F. M. Smulders, "Statistical characterization of 60-GHz indoor radio channels," *IEEE Trans. Antennas Propag.*, vol. 57, no. 10, pp. 2820–2829, Oct. 2009.

[234] M. R. Akdeniz, Y. Liu, M. K. Samimi, S. Sun, S. Rangan, T. S. Rappaport, and E. Erkip, "Millimeter wave channel modeling and cellular capacity evaluation," *IEEE J. Sel. Areas Commun.*, vol. 32, no. 6, pp. 1164–1179, Jun. 2013.

[235] C. Gustafson, K. Haneda, S. Wyne, and F. Tufvesson, "On mm-wave multipath clustering and channel modeling," *IEEE Trans. Antennas Propag.*, vol. 62, no. 3, pp. 1445–1455, Mar. 2014.

[236] J.-H. Park, Y. Kim, Y.-S. Hur, K. Lim, and K.-H. Kim, "Analysis of 60 GHz band indoor wireless channels with channel configurations," in *Proc. 9th IEEE Int. Symp. Pers., Indoor Mobile Radio Commun.*, vol. 2, Sep. 1998, pp. 617–620.

[237] J. Kunisch, E. Zollinger, J. Pamp, and A. Winkelmann, "MEDIAN 60 GHz wideband indoor radio channel measurements and model," in *Proc. Gateway to 21st Century Commun. Village (VTC-Fall) IEEE VTS 50th Veh. Technol. Conf.*, vol. 4, Sep. 1999, pp. 2393–2397.

[238] S. Reynaud, Y. Cocheril, R. Vauzelle, C. Guiffaut, and A. Reineix, "Hybrid FDTD/UTD indoor channel Modeling. Application to WiFi transmission systems," in *Proc. IEEE Veh. Technol. Conf.*, Sep. 2006, pp. 1–5.

[239] M. Thiel and K. Sarabandi, "A hybrid method for indoor wave propagation modeling," *IEEE Trans. Antennas Propag.*, vol. 56, no. 8, pp. 2703–2709, Aug. 2008.

[240] A. Molisch, M. Steinbauer, and H. Asplund, "'Virtual cell deployment areas' and 'cluster tracing'—New methods for directional channel modeling in microcells," in *Proc. Veh. Technol. Conf. IEEE 55th Veh. Technol. Conf. (VTC Spring)*, vol. 3, May 2002, pp. 1279–1283.

[241] L. Liu, C. Oestges, J. Poutanen, K. Haneda, P. Vainikainen, F. Quitin, F. Tufvesson, and P. D. Doncker, "The COST 2100 MIMO channel model," *IEEE Wireless Commun.*, vol. 19, no. 6, pp. 92–99, Dec. 2012.

[242] R. J. Weiler, M. Peter, W. Keusgen, A. Maltsev, I. Karls, A. Pudeyev, I. Bolotin, I. Siaud, and A.-M. Ulmer-Moll, "Quasi-deterministic millimeter-wave channel models in MiWEBA," *EURASIP J. Wireless Commun. Netw.*, vol. 2016, no. 1, Dec. 2016, Art. no. 84.

[243] M. Lecci, M. Polese, C. Lai, J. Wang, C. Gentile, N. Golmie, and M. Zorzi, "Quasi-deterministic channel model for mmWaves: Mathematical formalization and validation," in *Proc. IEEE Global Commun. Conf.*, Dec. 2020, pp. 1–6.

[244] A. Maltsev, A. Pudeyev, I. Karls, I. Bolotin, G. Morozov, R. Weiler, M. Peter, and W. Keusgen, "Quasi-deterministic approach to mmWave channel modeling in a non-stationary environment," in *Proc. IEEE Globecom Workshops (GC Wkshps)*, Dec. 2014, pp. 966–971.

[245] Q. Zhu, C.-X. Wang, B. Hua, K. Mao, S. Jiang, and M. Yao, *3GPP TR 38.901 Channel Model*. Hoboken, NJ, USA: Wiley, 2021, pp. 1–35. [Online]. Available: https://onlinelibrary.wiley.com/doi/abs/10.1002/9781119471509.w5GRef048

[246] J. Feng, L. Zhou, X. Xu, and C. Liao, "A hybrid TDPE/FDTD method for site-specific modeling of O2I radio wave propagation," *IEEE Antennas Wireless Propag. Lett.*, vol. 17, no. 9, pp. 1652–1655, Sep. 2018.

[247] M. Kim, T. Iwata, S. Sasaki, and J.-I. Takada, "Millimeter-wave radio channel characterization using multi-dimensional sub-grid CLEAN algorithm," *IEICE Trans. Commun.*, vol. E103.B, no. 7, pp. 767–779, 2020.

[248] P. Kyösti, J. Meinilä, L. Hentilä, X. Zhao, T. Jämsä, C. Schneider, M. Narandzic, M. Milojevic, A. Hong, J. Ylitalo, V.-M. Holappa, M. Alatossava, R. Bultitude, Y. D. Jong, and T. Rautiainen, "IST-4–027756 WINNER II D1.1.2 V1.2 WINNER II channel models," Inf. Soc. Technol., Ankara, Turkey, Tech. Rep. D1.1.2, Version 1.2, 2008.

[249] *Study on 3D Channel Model for LTE*, document 36.873, 3rd Generation Partnership Project (3GPP), 2018.

[250] J. Kunisch and J. Pamp, "An ultra-wideband space-variant multipath indoor radio channel model," in *Proc. IEEE Conf. Ultra Wideband Syst. Technol.*, Nov. 2003, pp. 290–294.

[251] A. Maltsev, R. Maslennikov, A. Sevastyanov, A. Lomayev, and A. Khoryaev, "Statistical channel model for 60 GHz WLAN systems in conference room environment," in *Proc. 4th Eur. Conf. Antennas Propag.*, 2010, pp. 1–5.

[252] A. Maltsev, A. Pudeyev, A. Lomayev, and I. Bolotin, "Channel modeling in the next generation mmWave Wi-Fi: IEEE 802.11ay standard," in *Proc. 22th Eur. Wireless Conf.*, 2016, pp. 1–8.

[253] G. R. MacCartney, H. Yan, S. Sun, and T. S. Rappaport, "A flexible wideband millimeter-wave channel sounder with local area and NLOS to LOS transition measurements," in *Proc. IEEE Int. Conf. Commun. (ICC)*, May 2017, pp. 1–7.

[254] K. Sengupta and A. Hajimiri, "A 0.28 THz power-generation and beam-steering array in CMOS based on distributed active radiators," *IEEE J. Solid-State Circuits*, vol. 47, no. 12, pp. 3013–3031, Dec. 2012.

[255] Y. Tousi and E. Afshari, "A high-power and scalable 2-D phased array for terahertz CMOS integrated systems," *IEEE J. Solid-State Circuits*, vol. 50, no. 2, pp. 597–609, Feb. 2015.

[256] K. Sengupta and A. Hajimiri, "Mutual synchronization for power generation and beam-steering in CMOS with on-chip sense antennas near 200 GHz," *IEEE Trans. Microw. Theory Tech.*, vol. 63, no. 9, pp. 2867–2876, Sep. 2015.

[257] A. Simsek, A. S. H. Ahmed, A. A. Farid, U. Soylu, and M. J. W. Rodwell, "A 140 GHz two-channel CMOS transmitter using low-cost packaging technologies," in *Proc. IEEE Wireless Commun. Netw. Conf. Workshops (WCNCW)*, Apr. 2020, pp. 1–3.

[258] A. Gupta, M. Medley, and J. M. Jornet, "Joint synchronization and symbol detection design for pulse-based communications in the THz band," in *Proc. IEEE Global Commun. Conf. (GLOBECOM)*, Dec. 2015, pp. 1–7.

[259] Q. Xia, Z. Hossain, M. Medley, and J. M. Jornet, "A link-layer synchronization and medium access control protocol for terahertz-band communication networks," *IEEE Trans. Mobile Comput.*, vol. 20, no. 1, pp. 2–18, Jan. 2021.

[260] A. Agarwal, A. S. Sengar, and S. Debnath, "A novel noise floor estimation technique for optimized thresholding in spectrum sensing," in *Proc. Int. Conf. Adv. Comput., Commun. Informat. (ICACCI)*, Sep. 2017, pp. 607–611.

[261] D. Dupleich, R. Müller, and R. Thoma, "Practical aspects on the noise floor estimation and cut-off margin in channel sounding applications," in *Proc. 15th Eur. Conf. Antennas Propag. (EuCAP)*, Mar. 2021, pp. 1–5.

[262] S. Chinchali, A. Sharma, J. Harrison, A. Elhafsi, D. Kang, E. Pergament, E. Cidon, S. Katti, and M. Pavone, "Network offloading policies for cloud robotics: A learning-based approach," *Auto. Robots*, vol. 45, no. 7, pp. 997–1012, Oct. 2021.

[263] M. Chen, Y. Tian, G. Fortino, J. Zhang, and I. Humar, "Cognitive Internet of Vehicles," *Comput. Commun.*, vol. 120, pp. 58–70, May 2018. [Online]. Available: https://www.sciencedirect.com/science/article/pii/S0140366417311015
[264] M. Aladsani, A. Alkhateeb, and G. C. Trichopoulos, "Leveraging mmWave imaging and communications for simultaneous localization and mapping," in *Proc. IEEE Int. Conf. Acoust., Speech Signal Process. (ICASSP)*, May 2019, pp. 4539–4543.
[265] X.-F. Teng, Y.-T. Zhang, C. C. Y. Poon, and P. Bonato, "Wearable medical systems for p-health," *IEEE Rev. Biomed. Eng.*, vol. 1, pp. 62–74, 2008.
[266] T. Rappaport, Y. Xing, G. R. MacCartney, A. F. Molisch, E. Mellios, and J. Zhang, "Overview of millimeter wave communications for fifth-generation (5G) wireless networks-with a focus on propagation models," *IEEE Trans. Antennas Propag.*, vol. 65, no. 12, pp. 6213–6230, Dec. 2017.
[267] V. Petrov, A. Pyattaev, D. Moltchanov, and Y. Koucheryavy, "Terahertz band communications: Applications, research challenges, and standardization activities," in *Proc. 8th Int. Congr. Ultra Modern Telecommun. Control Syst. Workshops (ICUMT)*, Oct. 2016, pp. 183–190.
[268] *Study on Channel Model for Frequencies From 0.5 to 100 GHz (Release 14)*, document 38.901, 3rd Generation Partnership Project (3GPP), 2017. [Online]. Available: http://www.3gpp.org/DynaReport/38901.htm
[269] M. Mozaffari, A. T. Z. Kasgari, W. Saad, M. Bennis, and M. Debbah, "Beyond 5G with UAVs: Foundations of a 3d wireless cellular network," *IEEE Trans. Wireless Commun.*, vol. 18, no. 1, pp. 357–372, Jan. 2019.
[270] S. Hu, F. Rusek, and O. Edfors, "Beyond massive MIMO: The potential of data transmission with large intelligent surfaces," *IEEE Trans. Signal Process.*, vol. 66, no. 10, pp. 2746–2758, May 2018.
[271] V. V. Ratnam, H. Chen, S. Pawar, B. Zhang, C. J. Zhang, Y.-J. Kim, S. Lee, M. Cho, and S.-R. Yoon, "FadeNet: Deep learning-based mm-wave large-scale channel fading prediction and its applications," *IEEE Access*, vol. 9, pp. 3278–3290, 2021.
[272] E. Ostlin, H.-J. Zepernick, and H. Suzuki, "Macrocell path-loss prediction using artificial neural networks," *IEEE Trans. Veh. Technol.*, vol. 59, no. 6, pp. 2735–2747, Jul. 2010.
[273] R. He, B. Ai, A. F. Molisch, G. L. Stuber, Q. Li, Z. Zhong, and J. Yu, "Clustering enabled wireless channel modeling using big data algorithms," *IEEE Commun. Mag.*, vol. 56, no. 5, pp. 177–183, May 2018.
[274] F. Ademaj, M. K. Mueller, S. Schwarz, and M. Rupp, "Modeling of spatially correlated geometry-based stochastic channels," in *Proc. IEEE 86th Veh. Technol. Conf. (VTC-Fall)*, Sep. 2017, pp. 1–6.
[275] Y. Wang et al., "5G channel model for bands up to 100 GHz," in *Proc. Int. Workshop Wireless Positioning Navigat. (WPN)*. Espoo, Finland: Aalto Univ., 2016, pp. 1–107. [Online]. Available: http://www.5gworkshops.com/5GCM.html

ANIRBAN GHOSH (Member, IEEE) received the bachelor's degree from Jadavpur University, Kolkata, India, in 2010, the master's degree from the National Institute of Technology, Durgapur, India, in 2012, and the Ph.D. degree from North Dakota State University, Fargo, ND, USA, in 2018.

He worked as an Assistant Professor with KIIT University, Bhubaneswar, India, in 2012; and as a Wireless System Engineer with Clifton Technologies LLC, USA, in 2018. He is currently a specially appointed Assistant Professor with Niigata University, Japan, and he is on deputation as an Assistant Professor from SRM University AP, Andhra Pradesh, India. While working with Clifton Technologies LLC, he was a part of the team that deployed the patented 220 MHz IoT network. His current research interests include secrecy capacity determination using information theory, the various IoT applications and solutions, channel measurement and modeling, and biomedical image processing.

MINSEOK KIM (Senior Member, IEEE) was born in Seoul, South Korea. He received the B.S. degree in electrical engineering from Hanyang University, Seoul, in 1999, and the M.E. and D.E. degrees from the Division of Electrical and Computer Engineering, Yokohama National University (YNU), Japan, in 2002 and 2005, respectively. In 2007, he was an Assistant Professor with the Tokyo Institute of Technology, Tokyo, Japan, and a Visiting Scholar with the Georgia Institute of Technology, Atlanta, GA, USA, in 2010. In 2014, he joined the Graduate School of Engineering, Niigata University, Niigata, Japan, as an Associate Professor. His current research interests include radio propagation channel measurement and modeling, terahertz/millimeter-wave radar, radio tomographic imaging techniques, and MIMO/antenna array signal processing. He is a Senior Member of the IEICE. He is also serving as an Associate Editor for IEEE Access.